

Author's response by Wenjie Wang et al.

Corresponding to [li\\_xin@pku.edu.cn](mailto:li_xin@pku.edu.cn).

We greatly appreciate the time and efforts that the Referees spent in reviewing our manuscript. The comments are really thoughtful and helpful to improve the quality of our paper. We have addressed each comment below, with the Referee comment in black text, our response in blue text, and relevant manuscript changes noted in red text.

-----

### **Referee #1**

1. There is gap between ozone production and its concentration. A recent ACPD paper (Gao J.H. et al., doi:10.5194/acp-2020-140) and also references in the second paragraph of their Introduction Section highlighted that decreased ozone production by PM<sub>2.5</sub> via affecting photolysis rates is much more than the reduction in surface ozone concentration. Moreover, a lot of different transport model studies (Xing J. et al., doi:10.5194/acp-17-9869-2017; Li J. et al. doi: 10.1016/j.scitotenv.2017.12.041; Li K. et al., doi:10.1038/s41561-019-0464-x) also show that the impact of PM<sub>2.5</sub> on summer surface ozone is not important. I suggest, at least, the authors to do some detailed discussion to reconcile this important issue. This is particularly helpful for future studies.

Response: I agree with you that there is gap between ozone production and its concentration. I have given some detailed discussion to reconcile this important issue.

Line 542 - 558: Several three-dimension transport model studies show that the impact of PM<sub>2.5</sub> on summer surface ozone is not important (Li et al., 2018;Li et al., 2019c;Li et al., 2019b;Xing et al., 2017). Moreover, a recent study highlighted that decreased ozone production by PM<sub>2.5</sub> via affecting photolysis rates is much more than the reduction in surface ozone concentration (Gao et al., 2020). The difference between the two reductions in ozone production and surface ozone concentration indicates that, in addition to ozone photochemistry, there must be other ozone related physical processes influenced by the reduction in photolysis rate induced by aerosols. Model simulation indicates that aerosols lead to high concentrations of ozone aloft being

entrained by turbulence from the top of the planetary boundary layer (PBL) to the surface by altering photolysis rate and partly counteracting the reduction in surface ozone photochemical production induced by aerosols. In addition, the impact of aerosols on ozone from local and adjacent regions was more significant than that from long-distance regions (Gao et al., 2020). The accurate quantification of the effects of vertical mixing and long-distance transport on surface ozone concentration plays a critical role in the impact of aerosols on surface ozone, which needs further study in the future.

---

2. Diurnal variation of ozone production. The authors take daytime average over 7:00-19:00 or (6:00-18:00?) for ozone production. I am not sure if the results may differ by narrowing the average to afternoon hours when ozone production is active and HOx levels are high. Also, Hollaway et al. (doi:10.5194/acp-19-9699-2019) show that PM2.5 impacts on the summertime photolysis of NO<sub>2</sub> and ozone level at surface in Beijing are important before 11 am and after 3 pm but very limited in afternoon hours. I suggest the authors to show some diurnal information of simulated ozone production.

Response: I have analyzed the trend of simulated P(O<sub>3</sub>) in the afternoon hour (12:00-15:00), which increased at a rate of 1.3% yr<sup>-1</sup>, lower than the increasing rate of daytime average P(O<sub>3</sub>). Diurnal variation of simulated P(O<sub>3</sub>) in 2013 is shown in Figure S1. The diurnal variation of simulated P(O<sub>3</sub>) in this study indicates that the influence of aerosols on P(O<sub>3</sub>) is still significant in the afternoon leading to P(O<sub>3</sub>) decreased by ~17%, which is slightly lower than the decrease in the whole daytime (25%) (Figure S2). This is because that the average AOD in the afternoon (1.4) is significantly higher than that before 11:00 am (0.94) and after 3:00 pm (1.1) despite lower SZA and lower light absorptive ability (i.e. higher SSA) in the afternoon.

Line 461-472: The simulated P(O<sub>3</sub>) in the afternoon hour (12:00-15:00) when ozone production is active and HOx levels are high increased at a rate of 1.3% yr<sup>-1</sup>, which is lower than the increasing rate of daytime average P(O<sub>3</sub>) (2.2% yr<sup>-1</sup>) (Figure S2).

Hollaway et al. (2019) show that the impacts of aerosols on the summertime

photolysis of NO<sub>2</sub> and ozone at surface in Beijing are important before 11:00 am and after 3:00 pm but very limited in afternoon hours due to lower SZA and lower light absorptive ability of aerosol in the afternoon. However, the diurnal variation of simulated P(O<sub>3</sub>) in this study indicates that the influence of aerosols on P(O<sub>3</sub>) is still significant in the afternoon leading to P(O<sub>3</sub>) decreased by ~17%, which is slightly lower than the decrease in the whole daytime (25%) (Figure S3). This is because that the average AOD in the afternoon (1.4) is significantly higher than that before 11:00 am (0.94) and after 3:00 pm (1.1) despite lower SZA and lower light absorptive ability (i.e. higher SSA) in the afternoon.

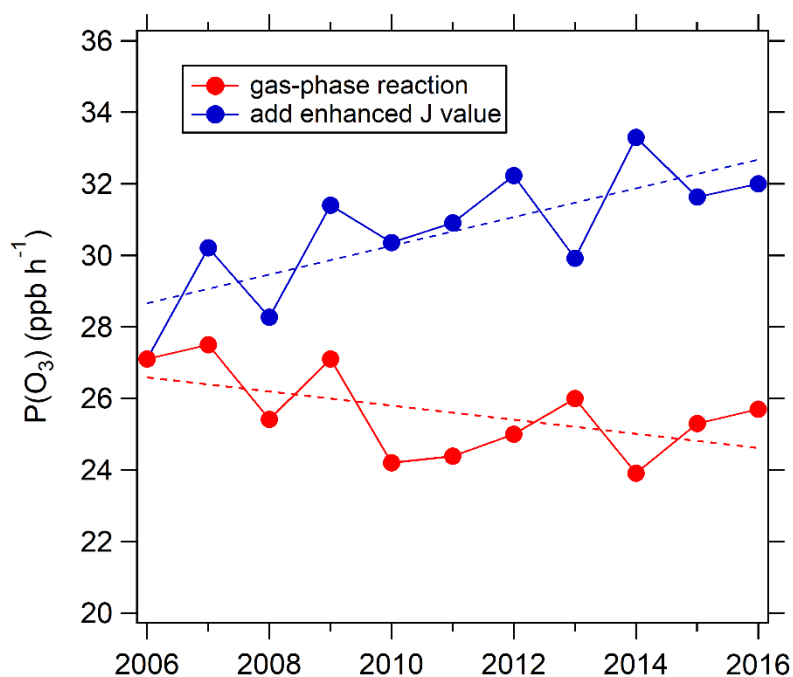


Figure S2. Trend of monthly afternoon (12:00-15:00) mean P(O<sub>3</sub>) simulated by the chemical box model. Red dots: Only the gas-phase reactions are considered in the box model constrained by observed photolysis frequencies from 2006 for all eleven years. Blue dots: the box model as above, but constrained by the photolysis frequencies derived for each year.

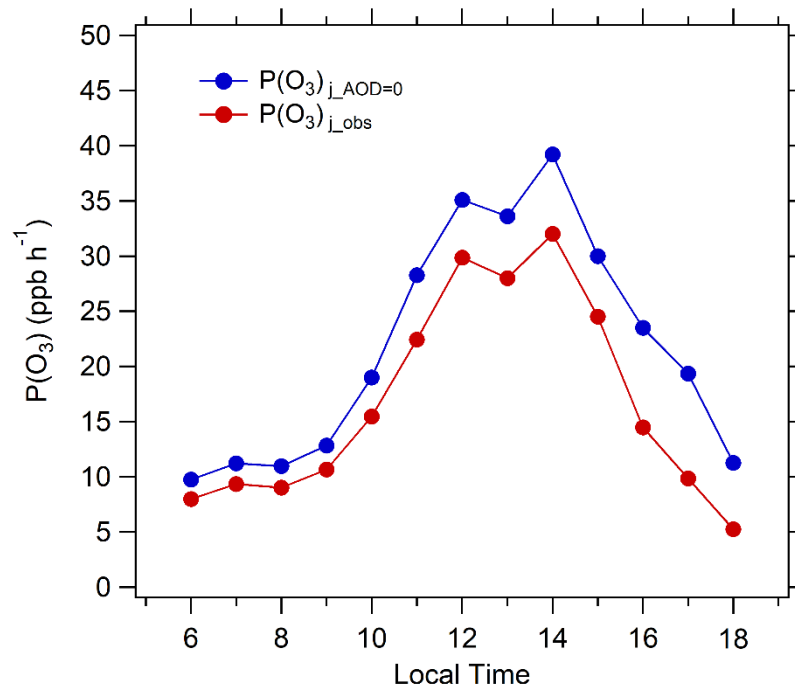


Figure S3. Diurnal variation of simulated  $P(O_3)$  in Beijing in August during 2005-2016.  $P(O_3)_{j_{obs}}$  represents ozone production rate under observed photolysis frequencies;  $P(O_3)_{j_{AOD=0}}$  represents ozone production rate under calculated photolysis frequencies when AOD is equal to 0.

---

3. The authors show an important result of an increased SSA in Beijing (Fig.12). More importantly, there is a shift pattern of  $j(NO_2)$  over 2006-2016 that the crossing point between  $J(NO_2)$  profile of 2006 and zero AOD profile changed from above PBL to below PBL in 2016. I think this means that the role of PM<sub>2.5</sub> may be more important under condition like 2006, but will be limited under condition like 2016 when there is offsetting effect for PBL ozone by vertical mixing. This may deserve a discussion.

Response: Yes, I agree with you. This is a good point. I have given a brief discussion according to your suggestion.

Line 533-541: However, there is a shift in the vertical profile of  $j(NO_2)$  that is important. The crossing point between  $j(NO_2)$  profile of 2006 and zero AOD profile is below PBL, while in 2016 the  $j(NO_2)$  profile crosses the zero AOD profile within the PBL. This means that as the AOD is reduced further, changes in the vertical average

$j(\text{NO}_2)$  will be limited, since increases in  $j(\text{NO}_2)$  near the top of the PBL will compensate for decreases near the surface. Additionally, this also denotes that the role of  $\text{PM}_{2.5}$  may be more important under condition like 2006, but will be limited under condition like 2016 when there is offsetting effect for PBL ozone by vertical mixing caused by larger ozone vertical gradient (Gao et al., 2020).

---

4. Some other specific comments. (1) It is confused to see 2005-2016 and 2006-2016 in the text. Please clarify this. (2) I suggest to use p-value other than the r square where there is a trend analysis. (3) Line 290: Shanghai should be “the south to North China Plain”. (4) Lines 293-296: how about the role of regional contribution outside of Beijing? For example, the increasing emissions in the whole North China Plain. (5) Line 494: Please take caution when saying “ozone increase”. you mean surface ozone concentrations?

Response: (1)  $\text{NO}_x$  data in 2005 were not available. Therefore, the trend of  $\text{NO}_x$  during 2006-2016 was analyzed. In addition, we focus on the trend of  $\text{P}(\text{O}_3)$  during the period of 2006-2016 due to the lack of  $\text{NO}_x$  data in 2005. (2) Thank you. I have summarized p-values for the temporal trend of all parameters in table 2. (3) Thank you. I have revised it. (4) In this study, we mainly focus on the variation of the local ozone production. It is difficult to give an accurate estimation of the regional contribution outside of Beijing. Previous studies have reported that regional transport from neighboring provinces outside Beijing (including Hebei, Tianjin and Shandong) contributed about 35%-60% of ozone in Beijing during high ozone episodes (Streets et al., 2007; Wang et al., 2020). I have analyzed the ozone trend in Changdao site, a background site in the east of North China Plain, to discuss the regional contribution outside of Beijing due to increasing emissions in the whole North China Plain. This site is nearly not influenced by local anthropogenic emissions. MDA8 ozone concentrations at the Changdao site increased slowly ( $+1.2 \text{ ppbv yr}^{-1}$ ,  $r^2 = 0.11$ ,  $p=0.25$ ) during 2013-2019, which is about a half of the increasing rate of MDA8 ozone concentrations at PKUER site ( $+2.3 \pm 1.2 \text{ ppbv yr}^{-1}$ ,  $r^2=0.66$ ) during 2006-2016.

345-346: NO<sub>x</sub> data in 2005 were not available. Therefore, the trend of NO<sub>x</sub> during 2006-2016 was analyzed.

438-439: We focus on the period during 2006-2016 due to the lack of NO<sub>x</sub> data in 2005.

Line 657-658:

Table 2. p value of temporal trends for different parameters.

Parameter	Period	r <sup>2</sup>	p value	P value <0.01?	P value <0.05?
median	2005-2016	0.63	0.002	yes	yes
perc98	2005-2016	0.11	0.288	no	no
DTAvg	2005-2016	0.47	0.014	no	yes
MDA1	2005-2016	0.32	0.057	no	no
MDA8	2005-2016	0.66	0.001	yes	yes
4MDA8	2005-2016	0.42	0.023	no	yes
AOT40	2005-2016	0.67	0.001	yes	yes
NDGT70	2005-2016	0.56	0.005	yes	yes
SOMO35	2005-2016	0.57	0.004	yes	yes
exceedance	2005-2016	0.32	0.054	no	no
Ox	2005-2016	0.38	0.044	no	yes
CO	2005-2016	0.87	0.001	yes	yes
VOC reactivity	2005-2016	0.52	0.006	yes	yes
NO <sub>x</sub>	2006-2016	0.81	0.001	yes	yes
Calculated j(NO <sub>2</sub> )	2006-2016	0.94	0.000	yes	yes
AOD (380 nm)	2006-2016	0.78	0.000	yes	yes
PM <sub>2.5</sub>	2009-2016	0.93	0.000	yes	yes
Sa	2006-2016	0.51	0.010	yes	yes
SSA	2005-2016	0.70	0.001	yes	yes
AE	2005-2016	0.03	0.593	no	no
COT	2005-2016	0.003	0.875	no	no
Total O <sub>3</sub> column	2005-2016	0.15	0.215	no	no

Line 307-309: Additionally, there were very small trends of O<sub>3</sub> concentrations at the background site (Dongtan) in Shanghai, located to the south of the North China Plain (Gao et al., 2017).

Line 309-317: However, these background sites in Beijing and Shanghai may be strongly affected by local emissions. MDA8 ozone concentrations at the Changdao site, a background site in the east of the North China Plain that is much less

influenced by local emissions, increased slowly ( $+1.2 \text{ ppbv yr}^{-1}$ ,  $r^2=0.11$ ), but that rate is not statistically significant ( $p = 0.25$ ) during 2013-2019 (Figure S1). Based on these reports of smaller and variable trends, we assume that the trend in regional background ozone in the North China Plain made only a minor contribution to the relatively larger ozone trend observed at the PKUERS site ( $+2.3 \pm 1.2 \text{ ppbv yr}^{-1}$ ,  $r^2=0.66$ ,  $p = 0.001$ ).

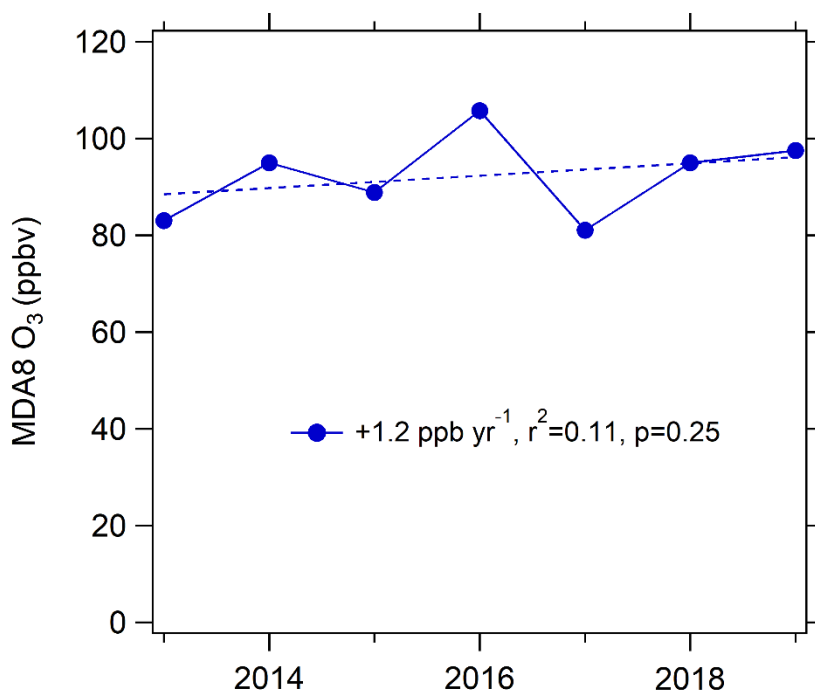


Figure S1. The trend of average MDA8 ozone in Changdao during 2013-2019. These data is acquired from “Blue book on prevention and control of atmospheric ozone pollution in China (in Chinese)” reported by Chinese Society of Environmental Sciences in 2020 ([http://www.epserve.com/forepart/zxnr\\_index.do?oid=51478637&tid=26378242](http://www.epserve.com/forepart/zxnr_index.do?oid=51478637&tid=26378242)).

---

## Referee #2

1. Regional transport is also a key source of surface ozone. This work tried to assess the impact of regional O<sub>3</sub> by analyzing measurements at a regional background site. This is not sufficient because this site was largely affected by Beijing emissions. I suggested that other background sites can be employed or backtransjectories at typical year can be used to analyze the impact of regional transport.

Response: I agree with you that the regional background site in Beijing was largely affected by Beijing emissions. I have chosen another site in Changdao, Shandong province, which is nearly not influenced by local emissions and thus is a better background site in North China Plain. MDA8 ozone concentration at the Changdao site increased at a rate of 1.2 ppbv yr<sup>-1</sup> ( $r^2=0.11$ ) during 2013-2019, which is significantly smaller than that at PKUER site during 2006-2016 (2.3 ppbv yr<sup>-1</sup>,  $r^2=0.66$ ) and during 2013-2019 (2.0 ppbv yr<sup>-1</sup>,  $r^2=0.67$ ).

Line 309-317: However, these background sites in Beijing and Shanghai may be strongly affected by local emissions. MDA8 ozone concentrations at the Changdao site, a background site in the east of the North China Plain that is much less influenced by local emissions, increased slowly (+1.2 ppbv yr<sup>-1</sup>,  $r^2=0.11$ ), but that rate is not statistically significant ( $p = 0.25$ ) during 2013-2019 (Figure S1). Based on these reports of smaller and variable trends, we assume that the trend in regional background ozone in the North China Plain made only a minor contribution to the relatively larger ozone trend observed at the PKUERS site ( $+2.3 \pm 1.2$  ppbv yr<sup>-1</sup>,  $r^2=0.66$ ,  $p = 0.001$ ).

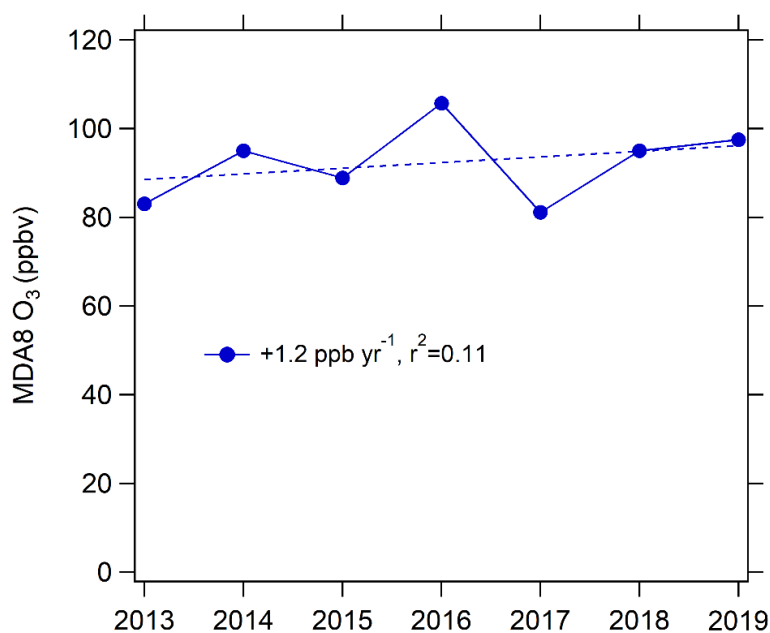


Figure S1. The trend of average MDA8 ozone in Changdao during 2013-2019. These data is from “Blue book on prevention and control of atmospheric ozone pollution in China (in Chinese)” reported by Chinese Society of Environmental Sciences in 2020 ([http://www.epserve.com/forepart/zxnr\\_index.do?oid=51478637&tid=26378242](http://www.epserve.com/forepart/zxnr_index.do?oid=51478637&tid=26378242)).

2. Recent, a few heterogeneous chemical reactions are thought to be potential factors of ozone. For example, photolysis of HNO<sub>3</sub> (NO<sub>3</sub><sup>-</sup>) adsorbed on the solid surface of aerosol particles effectively produces HONO and NO<sub>x</sub> in the gas phase (Salgado and Rossi et al., PCCP,2002; Ramazan, 2006). A short discuss should be performed.

Response: Thank you! I agree with you that A few heterogeneous chemical reactions of nitrogen oxides are thought to be potential influential factors of ozone production. I have added heterogeneous uptake of N<sub>2</sub>O<sub>5</sub>, NO<sub>2</sub> and NO<sub>3</sub> in the chemical box model to test its effect on ozone production. Our simulation indicates that the reduced heterogeneous uptake of NO<sub>x</sub> caused P(O<sub>3</sub>) to increase by only ~2.5 % during 2006-2016.

Line 249-253: Heterogeneous uptake of N<sub>2</sub>O<sub>5</sub>, NO<sub>2</sub> and NO<sub>3</sub> was included in the chemical box model. This includes  $\gamma_{N_2O_5} = 0.007$  for converting N<sub>2</sub>O<sub>5</sub> to HNO<sub>3</sub> (Wang et al., 2017),  $\gamma_{NO_2} = 1 \times 10^{-5}$  for conversion of NO<sub>2</sub> to HONO and HNO<sub>3</sub> (which yields a good simulation of HONO/NO<sub>2</sub> concentration ratios in China (Shah et al., 2020)) and  $\gamma_{NO_3} = 1 \times 10^{-3}$  for conversion of NO<sub>3</sub> to HNO<sub>3</sub> (Jacob, 2000).

Line 487-495: A few heterogeneous chemical reactions of nitrogen oxides are thought to be potential influential factors of ozone production. For example, the heterogeneous uptake of NO<sub>2</sub> to produce HNO<sub>3</sub> and HONO, and the heterogeneous uptake of NO<sub>3</sub> and N<sub>2</sub>O<sub>5</sub> to produce HNO<sub>3</sub>. Our simulation indicates that the reduced heterogeneous uptake of NO<sub>x</sub> caused P(O<sub>3</sub>) to increase by only ~2.5 % during 2006-2016. K Li et al. [2019a] reported that the effect of heterogeneous uptake of nitrogen oxides on ozone is very small under VOC-limited and summertime conditions in North China Plain. Our simulated result in Beijing where is under VOC-limited and summertime conditions is consistent with the result of Li et al. [2019a].

#### Reference:

- Gao, J., Li, Y., Zhu, B., Hu, B., Wang, L., and Bao, F.: What have we missed when studying the impact of aerosols on surface ozone via changing photolysis rates?, *Atmos. Chem. Phys. Discuss.*, 2020, 1-28, 10.5194/acp-2020-140, 2020.
- Gao, W., Tie, X. X., Xu, J. M., Huang, R. J., Mao, X. Q., Zhou, G. Q., and Chang, L. Y.: Long-term trend of O<sub>3</sub> in a mega City (Shanghai), China: Characteristics, causes, and interactions with precursors, *Science of the Total Environment*, 603, 425-433, 10.1016/j.scitotenv.2017.06.099, 2017.
- Hollaway, M., Wild, O., Yang, T., Sun, Y., Xu, W., Xie, C., Whalley, L., Slater, E., Heard, D., and Liu, D.: Photochemical impacts of haze pollution in an urban environment, *Atmospheric Chemistry and Physics*, 19, 9699-9714, 2019.
- Jacob, D. J.: Heterogeneous chemistry and tropospheric ozone, *Atmos. Environ.*, 34, 2131-2159, 2000.
- Li, J., Chen, X. S., Wang, Z. F., Du, H. Y., Yang, W. Y., Sun, Y. L., Hu, B., Li, J. J., Wang, W., Wang, T., Fu, P. Q., and Huang, H. L.: Radiative and heterogeneous chemical effects of aerosols on ozone and inorganic aerosols over East Asia, *Science of the Total Environment*, 622, 1327-1342, 10.1016/j.scitotenv.2017.12.041, 2018.
- Li, K., Jacob, D. J., Liao, H., Shen, L., Zhang, Q., and Bates, K. H.: Anthropogenic drivers of 2013–2017 trends in summer surface ozone in China, *Proceedings of the National Academy of Sciences*, 116, 422-427, 2019a.
- Li, K., Jacob, D. J., Liao, H., Zhu, J., Shah, V., Shen, L., Bates, K. H., Zhang, Q., and Zhai, S.: A two-pollutant strategy for improving ozone and particulate air quality in China, *Nature Geoscience*, 12, 906-910, 10.1038/s41561-019-0464-x, 2019b.
- Shah, V., Jacob, D., Li, K., Silvern, R., Zhai, S., Liu, M., Lin, J., and Zhang, Q.: Effect of changing NO<sub>x</sub> lifetime on the seasonality and long-term trends of satellite-observed tropospheric NO<sub>2</sub> columns over China, 2020.

- Streets, D. G., Fu, J. S., Jang, C. J., Hao, J. M., and Yu, C.: Air quality during the 2008 Beijing Olympic Games, *Atmospheric Environment* (1967), 41, 4800-4492, 2007.
- Wang, H., Lu, K., Tan, Z., Sun, K., Li, X., Hu, M., Shao, M., Zeng, L., Zhu, T., and Zhang, Y.: Model simulation of NO<sub>3</sub>, N<sub>2</sub>O<sub>5</sub> and ClNO<sub>2</sub> at a rural site in Beijing during CAREBeijing-2006, *Atmospheric Research*, 196, 97-107, 2017.
- Wang, P., Wang, T., and Ying, Q.: Regional source apportionment of summertime ozone and its precursors in the megacities of Beijing and Shanghai using a source-oriented chemical transport model, *Atmos. Environ.*, 224, 10, 10.1016/j.atmosenv.2020.117337, 2020.
- Xing, J., Wang, J., Mathur, R., Wang, S., Sarwar, G., Pleim, J., Hogrefe, C., Zhang, Y., Jiang, J., and Wong, D. C.: Impacts of aerosol direct effects on tropospheric ozone through changes in atmospheric dynamics and photolysis rates, *Atmospheric chemistry and physics*, 17, 9869, 2017.

1 **Exploring the drivers of the increased ozone production in Beijing in**  
2 **summertime during 2005-2016**

3 Wenjie Wang<sup>1</sup>, David D. Parrish<sup>2</sup>, Xin Li<sup>1,3,4\*</sup>, Min Shao<sup>2,1</sup>, Ying Liu<sup>1</sup>, Sihua Lu<sup>1</sup>, Min  
4 Hu<sup>1</sup>, Yusheng Wu<sup>1,#</sup>, Limin Zeng<sup>1</sup>, Yuanhang Zhang<sup>1</sup>

5  
6  
7 <sup>1</sup> State Key Joint Laboratory of Environmental Simulation and Pollution Control,  
8 College of Environmental Sciences and Engineering, Peking University, Beijing,  
9 China

10 <sup>2</sup> Institute for Environmental and Climate Research, Jinan University,  
11 Guangzhou 511443, China

12 <sup>3</sup> International Joint Laboratory for Regional Pollution Control, Ministry of  
13 Education, Beijing, 100816, China

14 <sup>4</sup> Collaborative Innovation Centre of Atmospheric Environment and Equipment  
15 Technology, Nanjing University of Information Science & Technology, Nanjing,  
16 210044, China

17 <sup>#</sup> now at Department of Physics, University of Helsinki, Helsinki, Finland

18  
19  
20  
21  
22 \* Corresponding author.

23 Address: College of Environmental Sciences and Engineering, Peking  
24 University, Beijing 100871, China

25 Phone: 86-10-62757973

26 Email: [li\\_xin@pku.edu.cn](mailto:li_xin@pku.edu.cn)

27

28 **Abstract**

29 In the past decade, average PM<sub>2.5</sub> concentrations decreased rapidly under the  
30 strong pollution control measures in major cities in China; however, ozone (O<sub>3</sub>)  
31 pollution emerged as a significant problem. Here we examine a unique (for China) 12-  
32 year data set of ground-level O<sub>3</sub> and precursor concentrations collected at an urban site  
33 in Beijing (PKUERS), where the maximum daily 8 h average (MDA8) O<sub>3</sub> concentration  
34 and daytime Ox (O<sub>3</sub> + NO<sub>2</sub>) concentration in August increased by  $2.3 \pm 1.2$  ppbv ( $+3.3$   
35  $\pm 1.8\%$ ) yr<sup>-1</sup> and  $1.4 \pm 0.6$  ( $+1.9 \pm 0.8\%$ ) yr<sup>-1</sup> respectively from 2005 to 2016. In contrast,  
36 daytime concentrations of nitrogen oxides (NO<sub>x</sub>) and the OH reactivity of volatile  
37 organic compounds (VOCs) both decreased significantly. Over this same time, the  
38 decrease of particulate matter, and thus the aerosol optical depth, led to enhanced solar  
39 radiation and photolysis frequencies, with near-surface  $j(\text{NO}_2)$  increasing at a rate of  
40  $3.6 \pm 0.8\%$  yr<sup>-1</sup>. We use an observation based box model to analyze the combined effect  
41 of solar radiation and ozone precursor changes on ozone production rate, P(O<sub>3</sub>). The  
42 results indicate that the ratio of the rates of decrease of VOCs and NO<sub>x</sub> (about 1.1) is  
43 inefficient in reducing ozone production in Beijing. P(O<sub>3</sub>) increased during the decade  
44 due to more rapid atmospheric oxidation caused to a large extent by the decrease of  
45 particulate matter. This elevated ozone production was driven primarily by increased  
46 actinic flux due to PM<sub>2.5</sub> decrease and to a lesser extent by reduced heterogeneous  
47 uptake of HO<sub>2</sub>. Therefore, the influence of PM<sub>2.5</sub> on actinic flux and thus on the rate of  
48 oxidation of VOCs and NO<sub>x</sub> to ozone and to secondary aerosol (i.e., the major  
49 contributor to PM<sub>2.5</sub>) is important for determining the atmospheric effects of controlling  
50 the emissions of the common precursors of PM<sub>2.5</sub> and ozone when attempting to control  
51 these two important air pollutants.

52

53

54

## 55 **1 Introduction**

56 Tropospheric ozone (O<sub>3</sub>) plays a key role in the oxidizing capacity of the  
57 atmosphere and affects the global climate; high concentrations of ground-level ozone  
58 are harmful to human health and ecosystems (Monks et al., 2015;Fiore et al., 2009).  
59 Ozone is produced rapidly in sun-lit polluted air by photochemical oxidation of  
60 volatile organic compounds (VOCs) in the presence of nitrogen oxides (NO<sub>x</sub> ≡ NO +  
61 NO<sub>2</sub>) (Atkinson, 2000). In recent years, China has undergone rapid economic  
62 development, resulting in higher demand for energy, and greater usage of fossil fuels.  
63 As a result, high emissions to the atmosphere produce heavy pollution in eastern  
64 China, which now suffers from severe ozone pollution, especially in urban areas,  
65 where the daily maximum 8 h average (MDA8) ozone level often exceeds the  
66 standard of 80 ppb (Jinfeng et al., 2014;Wang et al., 2011;Zhang et al., 2014;Lu et al.,  
67 2018;Li et al., 2019a). A recent study reported that the national warm-season  
68 (April–September) fourth highest MDA8 ozone level (86.0 ppb) and the number of  
69 days with MDA8 values of > 70 ppb was much higher than regional averages in  
70 Japan, South Korea, Europe, or the United States (Lu et al., 2018). Satellite  
71 observations found that regional ozone concentrations in eastern China increased by  
72 7% between 2005 and 2010 (Verstraeten et al., 2015). From 2013 to 2017, the O<sub>3</sub>  
73 concentrations in 74 cities as a whole showed an upward trend with Beijing-Tianjin-  
74 Hebei region being the most serious (Li et al., 2019a;Lu et al., 2018). Better  
75 understanding of the causes of elevated ozone in China is important for developing  
76 effective emission control strategies to reduce the ozone pollution problem.

77 Aerosols impact ozone production primarily in two ways: alteration of photolysis  
78 rates by aerosol radiative influence and heterogeneous reactions occurring on the  
79 aerosol surface. The reduction of photolysis frequencies by the extinction effect of  
80 aerosol and thus its influence on ozone production has been explored in the past  
81 (Dickerson et al., 1997;Castro et al., 2001;Real and Sartelet, 2011;Gerasopoulos et al.,  
82 2012;Wang et al., 2019). Absorbing aerosols reduce photolysis frequencies

83 throughout the boundary layer, and as a result decrease near-surface photochemical  
84 ozone production (de Miranda et al., 2005; Jacobson, 1998; Wendisch et al., 1996; Raga  
85 et al., 2001). Conversely, scattering aerosols in the boundary layer increase photolysis  
86 frequencies throughout the troposphere, and thereby increase ozone production aloft  
87 (Jacobson, 1998; Tian et al., 2019; Dickerson et al., 1997). The importance of aerosol  
88 heterogeneous reactions in ozone photochemistry in China has been previously  
89 investigated in model studies (Lou et al., 2014; Li et al., 2018; Xu et al., 2012; Li et al.,  
90 2019a). The effects of NO<sub>2</sub>, NO<sub>3</sub>, and N<sub>2</sub>O<sub>5</sub> heterogeneous reactions showed opposite  
91 O<sub>3</sub> concentration changes in VOC-limited and NO<sub>x</sub>-limited regions. In a VOC-limited  
92 region, NO<sub>2</sub>, NO<sub>3</sub>, and N<sub>2</sub>O<sub>5</sub> heterogeneous reactions lead to ozone concentration  
93 increases (Lou et al., 2014; Xu et al., 2012). The heterogeneous reaction of HO<sub>2</sub>  
94 decreases ozone production in both VOC-limited and NO<sub>x</sub>-limited regions by  
95 decreasing the reaction rate of HO<sub>2</sub> with NO (Lou et al., 2014; Li et al., 2019a).

96 In the past decade, Eastern China has experienced severe fine particulate matter  
97 (PM<sub>2.5</sub>) pollution in winter (Zhang et al., 2016), and this issue has been the main focus  
98 of the government's air pollution control strategy. These stringent emission control  
99 measures have significantly decreased the concentrations of particulate matter in many  
100 Chinese cities. During 2008-2013, ground-level PM<sub>2.5</sub> estimated from satellite-  
101 retrieved aerosol optical depth (AOD) in China declined at a rate of 0.46 μg m<sup>-3</sup> year<sup>-1</sup>  
102 (Ma et al., 2016b). Another study indicated that the annual average concentration of  
103 PM<sub>2.5</sub> in Beijing decreased by 1.5 μg m<sup>-3</sup> year<sup>-1</sup> and 27% in total from 2000 to 2015  
104 under the implementation of 16 phases' air pollution control measures (Lang et al.,  
105 2017). Hu et al (2017) reported that PM<sub>2.5</sub> in Beijing declined significantly from 2006  
106 to 2016, and meanwhile solar radiation increased (Hu et al., 2017). However, despite  
107 the reduction in emissions of particulate matter (PM) and ozone precursors, ozone  
108 concentrations increased, even while PM concentrations decreased.

109 In Beijing, the second largest city in China, with rapid economic development and  
110 urbanization in recent years, ozone pollution is one of the worst among China's cities.  
111 Thus, Beijing is a representative city in which to study urban ozone pollution in China.  
112 Despite extensive study of the relationship between ozone and its precursors in Beijing

113 and other mega cities in China (Zhang et al., 2014;Chou et al., 2011;Lu et al., 2019;Liu  
114 et al., 2012), there remains a lack of understanding of the cause of the long-term [surface](#)  
115 [ozone concentration increase](#) that accompanied reductions in precursor emissions. In  
116 this study, we utilize measurements from a representative urban site in Beijing to  
117 explore how the variations in solar radiation and heterogeneous reactions influence the  
118 trend of ozone and the coupling effect of aerosol and ozone precursor changes on ozone  
119 production. Our overall goal is to determine the extent to which increasing actinic flux  
120 caused by the decline in PM contributed to the observed increase in ozone  
121 concentrations. This research provides a clearer understanding of how efforts to reduce  
122 PM concentrations affect ozone concentrations, and thus informs air quality  
123 improvement efforts in China's urban areas.

## 124 **2 Materials and methods**

### 125 2.1 Measurements of air pollutants, photolysis frequencies and aerosol surface 126 concentration

127 Ambient air pollutants and photolysis frequencies were measured at an urban site  
128 in Beijing in August between 2005 and 2016. The site (39.99° N, 116.31°E) was located  
129 on the roof of a six story building (~20m above the ground level) on the campus of  
130 Peking University (PKUERS) near the 4th Ring Road with high density of traffic, but  
131 without obvious industrial or agricultural sources (Wehner et al., 2008). Temporal  
132 trends of air pollutants and composition of VOCs are thought to be representative for  
133 the whole of Beijing (Wang et al., 2010;Xu et al., 2011;Zhang et al., 2012). Measured  
134 parameters include O<sub>3</sub>, NO<sub>x</sub>, CO, SO<sub>2</sub>, C<sub>2</sub> - C<sub>10</sub> VOCs, photolysis frequencies and  
135 aerosol surface concentration. The measurement techniques are included in the Table 1.

136 During 2006 and 2008, ambient levels of VOCs were measured using an online  
137 GC-FID system built by the Research Center for Environmental Changes (RCEC;  
138 Taiwan). A detailed description of this system and QA/QC procedures can be found in  
139 Wang et al. (Wang et al., 2004). During August 2007 and 2009, ambient VOCs were

140 measured using a commercial GC-FID/PID system (Syntech Spectra GC955 series  
141 600/800 analyzer) (Xie et al., 2008;Zhang et al., 2014). From 2010 to 2016, VOCs were  
142 measured using a cryogen-free online GC-MS/FID system developed by Peking  
143 University. A detailed description of this system and QA/QC procedures can be found  
144 in Yuan et al. and Wang et al. (Yuan et al., 2012;Wang et al., 2014). Formaldehyde  
145 (HCHO) concentrations were measured by a Hantzsch fluorimetry.

146 Photolysis frequencies (including  $j(\text{O}^1\text{D})$ ,  $j(\text{NO}_2)$ ,  $j(\text{HONO})$ ,  $j(\text{HCHO})_M$ ,  
147  $j(\text{HCHO})_R$ ,  $j(\text{H}_2\text{O}_2)$ ) were calculated from solar actinic flux spectra measured by a  
148 spectroradiometer as described by Bohn et al. (Bohn et al., 2008). The particle number  
149 size distributions were measured by a system consisting of a Nano-SMPS (TSI  
150 DMA3085 + CPC3776) and a SMPS (TSI DMA3081 + CPC3775). Aerosol surface  
151 concentration ( $S_a$ ) during 2006-2016 was calculated from the measured particle number  
152 size distributions between 3 nm and 700 nm by assuming the particles are spherical in  
153 shape.

## 154 2.2 Estimate of photolysis frequencies

155 Photolysis frequencies were measured in August 2011-2014 and 2016. The  
156 Tropospheric Ultraviolet and Visible (TUV) radiation model (version 5.3) was used to  
157 calculate photolysis frequencies in August over the entire 2006-2016 period under  
158 clear-sky conditions. TUV uses the discrete-ordinate algorithm (DISORT) with four  
159 streams and calculates the actinic flux spectra with a wavelength range of 280 – 420 nm  
160 in 1 nm steps and resolution. We used observed aerosol optical properties including  
161 AOD, single scattering albedo (SSA) and Ångström exponent (AE), total ozone column  
162 to constrain the TUV model (Madronich, 1993). The calculated values agree well with  
163 measured results as shown in Figure 1 indicating that the TUV model accurately  
164 calculated the photolysis frequencies. Data of photolysis frequencies under cloudless  
165 conditions were selected according to the presence of AOD data since AOD  
166 measurements were not possible under cloudy conditions.

## 167 2.3 Measurements of aerosol optical properties

168 Aerosol optical properties were measured with a CIMEL Sun photometer  
169 (AERONET level 1.5 and level 2.0 data collection, <http://aeronet.gsfc.nasa.gov/>) at the  
170 Beijing-CAMS site (39.933°N, 116.317°E) and at the Beijing site (39.977N,116.381E).  
171 The instrumentation, data acquisition, retrieval algorithms and calibration procedure,  
172 which conform to the standards of the AERONET global network, are described in  
173 detail by Fottiadi et al. (Fottiadi et al., 2006). The solar extinction measurements taken  
174 every 3 minutes within the spectral range 340 – 1020 nm were used to compute AOD  
175 at 340, 380, 440, 500, 675, 870, 970 and 1020 nm. The overall uncertainty in AOD data  
176 under cloud-free conditions was 0.02 at a wavelength of 440 nm (Dubovik and King,  
177 2000). In this study, AOD at the wavelength of 380nm was chosen for analysis. This  
178 wavelength was selected as it is more representative of  $j(\text{NO}_2)$ . In addition to AOD, that  
179 network also provided single scattering albedo (SSA) and Ångström exponent (AE)  
180 data.

181 Cloud optical thickness (COT) was acquired from Aura satellite measurements  
182 with a time resolution of 24 hours. Total ozone column was obtained by OMI (Ozone  
183 Monitoring Instrument), using overpass data.

## 184 2.4 Trend analysis method

185 A simple linear regression (the least-squares method) was implemented to  
186 investigate temporal trends of ozone, precursors, aerosol optical properties,  $\text{PM}_{2.5}$  and  
187 photolysis frequencies. The null hypothesis is that air pollutants and time have no  
188 linear relationship and this was tested using the standard F-statistic test (ratio of the  
189 mean-square regression to the mean-square residual). The p value associated with the  
190 F-statistic is the probability of mistakenly rejecting the null hypothesis (\*\*  $p < 0.01$ ; \*  
191  $p < 0.05$ ). The p values for the trends of different parameters are summarized in Table  
192 2.

## 193 2.5 Chemical box model

194 Ozone production rate,  $P(O_3)$ , is calculated by a chemical box model. This model  
195 is based on the compact Regional Atmospheric Chemical Mechanism version 2  
196 (RACM) described by Goliff et al. (Goliff et al., 2013), which includes 17 stable  
197 inorganic species, 4 inorganic intermediates, 55 stable organic compounds and 43  
198 intermediate organic compounds. Compounds that are not explicitly treated in the  
199 RACM are lumped into species with similar functional groups. The isoprene  
200 mechanism includes a more detailed mechanism based on the Leuven Isoprene  
201 Mechanism (LIM) proposed by Peeters et al. (Peeters et al., 2009). A detailed  
202 description of this model can be found in Tan et al. (Tan et al., 2017).

203 In this study, the model was constrained by measured hourly average CO, NO<sub>2</sub>,  
204 O<sub>3</sub>, SO<sub>2</sub>, NMHCs (56 species), HCHO, photolysis frequencies, temperature, pressure,  
205 and relative humidity. HONO was not measured. HONO concentrations are generally  
206 underestimated by the gas phase reaction source of HONO ( $OH + NO \rightarrow HONO$ ) in  
207 urban areas due to the emission of HONO and the heterogeneous reaction of NO<sub>x</sub> at  
208 surfaces to form HONO, both of which are related to NO<sub>x</sub> concentration. As a result,  
209 the HONO concentration was calculated according to the concentration of NO<sub>2</sub> and  
210 the observed ratio of HONO to NO<sub>2</sub> at an urban site in Beijing, which had a marked  
211 diurnal cycle (Hendrick et al., 2014). For the model calculation, the ratio of HONO to  
212 NO<sub>2</sub> is equal to 0.08 at 6:00 and decreases linearly from 0.08 to 0.01 during 6:00 -  
213 10:00 reflecting increasing photolysis of HONO, and maintains the value of 0.01  
214 during 10:00-18:00. In this study, we focused on daytime  $P(O_3)$  (6:00 - 18:00), thus  
215 the nocturnal HONO concentrations were not required.

216 RO<sub>2</sub>, HO<sub>2</sub>, OH were simulated by the box model to calculate the ozone  
217 production and loss rates as shown in Equations E1 and E2 as derived by Mihelcic et  
218 al. (Mihelcic et al., 2003).

$$219 \quad P(O_3) = k_{HO_2+NO} [HO_2][NO] + \sum (k^i_{RO_2+NO} [RO_2^i][NO]) - k_{OH+NO_2} [OH][NO_2] - L(O_3) \quad E1$$

$$220 \quad L(O_3) = (\theta j(O^1D) + k_{OH+O_3} [OH] + k_{HO_2+O_3} [HO_2] + \sum (k^j_{alkene+O_3} [alkene^j])) [O_3] \quad E2$$

221 where  $\theta$  is the fraction of O<sup>1</sup>D from ozone photolysis that reacts with water vapor.  $i$  and  
222  $j$  represent the number of species of RO<sub>2</sub> and alkenes, respectively.

223 The model runs were performed in a time-dependent mode with two days' spin-  
224 up. A 24 h lifetime was introduced for all simulated species, such as secondary species  
225 and radicals, to approximately simulate dry deposition and other losses of these  
226 species (Lu et al., 2013). This lifetime corresponds to an assumed deposition velocity  
227 of 1.2 cm s<sup>-1</sup> and a well-mixed boundary layer height of about 1 km. Sensitivity tests  
228 show that this assumed deposition lifetime has a relatively small influence on the  
229 reactivity of modeled oxidation products and RO<sub>x</sub> radicals.

230 Aerosols can influence O<sub>3</sub> production by heterogeneous reactions such as uptake  
231 of HO<sub>2</sub>, NO<sub>2</sub>, N<sub>2</sub>O<sub>5</sub> and NO<sub>3</sub>. For these species, the heterogeneous uptake of HO<sub>2</sub> is  
232 expected to have the largest effect on rapid ozone production in summertime and VOC-  
233 limited conditions (Li et al., 2019a). Thus, the effect of heterogeneous reaction of HO<sub>2</sub>  
234 on ozone production was simulated in the chemical box model using RH corrected  
235 aerosol surface concentration ( $S_{aw}$ ) and uptake coefficient of HO<sub>2</sub>. The rate of change  
236 in HO<sub>2</sub> due to irreversible uptake is expressed by E3.

$$237 \quad \frac{dC}{dt} = \frac{\gamma_{HO_2} \times S_{aw} \times v \times C}{4} \quad E3$$

238 Where  $C$ ,  $v$ , and  $\gamma_{HO_2}$  are the gas phase concentration, mean molecular velocity, and  
239 uptake coefficient, respectively. To derive  $S_{aw}$  we used the measured hygroscopic  
240 factor (Liu et al., 2009) and measured RH to correct the measurement-derived  $S_a$  to  
241 ambient conditions. In this study, we chose  $\gamma_{HO_2} = 0.2$  provided by laboratory  
242 measurements of HO<sub>2</sub> uptake by aerosol particles collected at two mountain sites in  
243 eastern China (Taketani et al., 2012). The effects of HO<sub>2</sub> uptake on P(O<sub>3</sub>) in Beijing in  
244 2006 were simulated assuming that the product of HO<sub>2</sub> uptake by aerosols is either  
245 H<sub>2</sub>O or H<sub>2</sub>O<sub>2</sub>. The results indicate that the two scenarios showed no significant  
246 difference because the recycling of HO<sub>x</sub> radicals from H<sub>2</sub>O<sub>2</sub> is inefficient (Li et al.,  
247 2019a). In the following simulations in this study, the product of HO<sub>2</sub> uptake by  
248 aerosols is taken to be H<sub>2</sub>O.

249 [Heterogeneous uptake of N<sub>2</sub>O<sub>5</sub>, NO<sub>2</sub> and NO<sub>3</sub> was included in the chemical box](#)

250 model. This includes  $\gamma_{\text{N}_2\text{O}_5} = 0.007$  for converting  $\text{N}_2\text{O}_5$  to  $\text{HNO}_3$  (Wang et al., 2017),  
251  $\gamma_{\text{NO}_2} = 1 \times 10^{-5}$  for conversion of  $\text{NO}_2$  to HONO and  $\text{HNO}_3$  (which yields a good  
252 simulation of HONO/ $\text{NO}_2$  concentration ratios in China (Shah et al., 2020)) and  $\gamma_{\text{NO}_3}$   
253  $= 1 \times 10^{-3}$  for conversion of  $\text{NO}_3$  to  $\text{HNO}_3$  (Jacob, 2000).

## 254 **3 Results and discussion**

### 255 3.1 Trend of ozone

256 Ozone pollution levels can be characterized by a number of metrics. Table 3 lists  
257 10 ozone metrics and their definition summarized by Lu et al. (2018). We classify these  
258 indicators into four categories: (1) metrics that characterize general levels of ozone:  
259 median value of hourly ozone concentrations (median), daily maximum 8 h average  
260 ozone concentration (MDA8) and daytime average ozone concentration (DTAvg); (2)  
261 metrics that characterize extreme levels of ozone: daily maximum 1 h average ozone  
262 concentration (MDA1), 98th percentile of hourly ozone concentrations (Perc98) and  
263 4th highest MDA8 (4MDA8); (3) metrics that characterize ozone exposure: cumulative  
264 hourly ozone concentrations of  $>40$  ppb (AOT40) and sum of positive differences  
265 between MDA8 and a cutoff concentration of 35 ppb (SOMO35); (4) The metrics that  
266 characterize the days when the ozone exceeds the standard: total number of days with  
267 MDA8 values of  $>70$  ppb (NDGT70) and number of days with the ozone concentration  
268 exceeding the Chinese grade II national air quality standard (Exceedance). Figure 2  
269 presents variations in these four categories of ozone metrics at PKUERS site during the  
270 study periods. The results show that overall all metrics increased during the 12 year  
271 period. However, the percent increase, the p value and the correlation coefficient vary  
272 between metrics. The median, DTAvg, and MDA8 indicators, which characterize the  
273 general concentration levels of ozone, increased at rates of 2.8% - 5.7%  $\text{yr}^{-1}$ . The  
274 metrics that characterize the extreme concentration levels of ozone increased more  
275 slowly (1.2% - 2.7%  $\text{yr}^{-1}$ ). Among them, Perc98 had the smallest rate of increase, only  
276 1.2%  $\text{yr}^{-1}$ , and the correlation is not significant ( $p = 0.29$ ,  $r^2 = 0.11$ ). This indicates that

277 increases in the extreme ozone pollution was less significant. In contrast, the increase  
278 rates of the ozone exposure metrics AOT40 and SOMO35 was are faster,  $8.4\% \text{ yr}^{-1}$  and  
279  $8.3\% \text{ yr}^{-1}$ , respectively, than the metrics that characterize ozone concentrations. The  
280 NDGT70 and Exceedance metrics, related to the number of days of ozone exceeding  
281 the standard, showed the fastest increases,  $10\% \text{ yr}^{-1}$  and  $9.8\% \text{ yr}^{-1}$ , respectively.

282 As shown in Figure 3, from 2005 to 2016 MDA8 O<sub>3</sub> concentrations increased at a  
283 rate of  $2.3 \pm 1.2 \text{ ppbv}$  ( $3.3 \pm 1.8 \%$ )  $\text{yr}^{-1}$  ( $r^2 = 0.66$ ) at the PKUERS site, which  
284 corresponds to a total MDA8 ozone concentration increase of 25.3 ppbv. Meanwhile,  
285 O<sub>x</sub> (O<sub>3</sub>+NO<sub>2</sub>) concentrations increased at a slower rate of  $1.4 \pm 0.6 \text{ ppbv}$  ( $1.9 \pm 0.8 \%$ )  
286  $\text{yr}^{-1}$ , due to the decrease in NO<sub>x</sub> concentrations (Figure 5).

287 Temperature and wind speed, which can directly influence ozone production and  
288 concentrations, showed no significant trend during 2005-2016 (Figure 4). The average  
289 temperatures in summer were between 26 and 31°C. The temperature in 2005 was the  
290 lowest and in 2007 it was the highest. The average wind speeds were less than  $2.5 \text{ m s}^{-1}$   
291 in all years. The average relative humidity may have decreased slightly ( $\sim 1.5\% \text{ yr}^{-1}$ ).  
292 In summary, we believe that meteorological factors did not play more than a minor role  
293 in the overall Beijing O<sub>3</sub> trend. Therefore, our discussion focuses on photochemical  
294 processes.

295 The ozone concentration observed at a receptor site depends on two  
296 contributions: regional background ozone and local photochemical production. We  
297 have no direct measurements of the long-term trend of regional background ozone in  
298 Beijing, but others have reported measurements of ozone at regional background sites  
299 in China. At a baseline Global Atmospheric Watch (GAW) station in the northeastern  
300 Tibetan Plateau region (Mt Waliguan, 36.28° N, 100.9° E) the average annual daytime  
301 ozone concentration increased at a rate of  $0.24 \text{ ppb yr}^{-1}$ , over the 1994 to 2013 period,  
302 but there was no significant trend in summer (Xu et al., 2018). The measurement at a  
303 rural station (Dingling site) in Beijing (116.22° E, 40.29° N, 34 km northwest of the  
304 observation site in this study) showed a decrease of ozone at a rate of  $-0.47 \text{ ppb yr}^{-1}$   
305 over the 2004 to 2015 period (Zheng et al., 2016). The MDA8 ozone concentration at

306 the Shangdianzi site, a background station in Beijing, showed an increasing trend of  
307 1.1 ppb yr<sup>-1</sup> during 2004-2014 (Ma et al., 2016a). Additionally, there were very small  
308 trends of O<sub>3</sub> concentrations at the background site (Dongtan) in Shanghai, located to  
309 the south of the North China Plain (Gao et al., 2017). However, these background  
310 sites in Beijing and Shanghai may be strongly affected by local emissions. MDA8  
311 ozone concentrations at the Changdao site, a background site in the east of the North  
312 China Plain that is much less influenced by local emissions, increased slowly (+1.2  
313 ppbv yr<sup>-1</sup>, r<sup>2</sup>=0.11), but that rate is not statistically significant (p = 0.25) during 2013-  
314 2019 (Figure S1). Based on these reports of smaller and variable trends, we assume  
315 that the trend in regional background ozone in the North China Plain made only a  
316 minor contribution to the relatively larger ozone trend observed at the PKUERS site  
317 (+2.3 ± 1.2 ppbv yr<sup>-1</sup>, r<sup>2</sup>=0.66, p = 0.001). We thus surmise that the increase in O<sub>3</sub> at  
318 the PKUERS site was mainly due to “local” photochemistry driven by emissions of  
319 ozone precursors from the central urban and surrounding suburban areas of Beijing.

### 320 **3.2 Trend of gaseous precursors**

321 This increase in ozone concentrations is opposite to the decreasing trend of its  
322 precursors, including VOCs, CO and NO<sub>x</sub> (Figure 5). The overall change of the total  
323 OH loss rate due to VOCs (VOC reactivity) was -0.36 s<sup>-1</sup> (-6.0%) yr<sup>-1</sup>. For  
324 anthropogenic VOCs, the highest reactivity was generally contributed by alkene  
325 species, with an average value over the eleven years of 2.00 ± 0.43 s<sup>-1</sup>, followed by  
326 aromatics and alkanes, with average reactivities of 1.51 ± 0.74 s<sup>-1</sup> and 0.92 ± 0.60 s<sup>-1</sup>,  
327 respectively. Thus, the alkenes and aromatics are more important for O<sub>3</sub> production  
328 than are alkanes. The trends for alkenes, aromatics, and alkanes were a decrease of  
329 0.14 s<sup>-1</sup> (7.1%), 0.12 s<sup>-1</sup> (7.9%), and 0.065s<sup>-1</sup> (7.0%) yr<sup>-1</sup>, respectively, indicating that  
330 alkenes and aromatics also played the dominant role in the reduction of anthropogenic  
331 VOC reactivity. The rate of decrease in VOCs at PKUERS site is similar to that  
332 reported for Los Angeles by Warneke et al. and Pollack et al. (7.3-7.5% yr<sup>-1</sup> over 50  
333 years) (Warneke et al., 2012;Pollack et al., 2013). The decrease in anthropogenic

334 VOCs in Los Angeles was predominantly attributed to decreasing emissions from  
335 motor vehicles due to increasingly strict emissions standards. Similarly, a previous  
336 study at the PKUERS site indicated that the decreasing anthropogenic VOC was  
337 mainly attributed to the reduction of gasoline evaporation and vehicular exhaust under  
338 the implementation of stricter emissions standards for new vehicles and specific  
339 control measures for in-use vehicles (Wang et al., 2015a). For naturally emitted  
340 VOCs, mainly isoprene, the OH reactivity had little trend with large fluctuations, as  
341 the emissions of plants vary greatly with temperature and light intensity. Therefore,  
342 the decrease in total VOCs reactivity was dominated by the decrease in anthropogenic  
343 VOCs. Similarly, CO, which is mainly contributed by anthropogenic emissions,  
344 decreased rapidly ( $9.3\% \text{ yr}^{-1}$ ) during 2006–2016.

345 [NOx data in 2005 were not available. Therefore, the trend of NOx during 2006-](#)  
346 [2016 was analyzed.](#) Daytime concentrations of NOx at the PKUER site also decreased  
347 significantly from 2006 to 2016 (Figure 5), with a slope (excluding 2008, which had a  
348 much lower NOx concentration due to enhanced emission controls implemented during  
349 the Olympic Games) of  $-1.48 \text{ ppbv yr}^{-1}$  ( $-5.5\% \text{ yr}^{-1}$ ,  $r^2 = 0.81$ ). The decrease in NOx  
350 was mainly due to the reduction in vehicle exhaust and coal combustion (Zhao et al.,  
351 2013). The decrease in NOx was significantly faster than that found in Los Angeles by  
352 Pollack et al. ( $2.6\% \text{ yr}^{-1}$  over 50 years) (Pollack et al., 2013). In contrast to Beijing, Los  
353 Angeles O<sub>3</sub> concentrations have continuously decreased from 1980 to 2010 (Parrish et  
354 al., 2016). The ratio of the rates of decrease of VOCs and NOx in Los Angeles (2.9) is  
355 significantly greater than unity and larger than that at the PKUER site (1.1), which  
356 possibly can be a contributing cause of the opposite trends of ozone in the two regions.  
357 It worth noting that the precursor concentrations in 2008, the Olympic Games year,  
358 were particularly low, but that ozone was nevertheless on the regression line. The  
359 monthly average ratio of VOC reactivity to NOx concentration in 2008 is  $0.28 \text{ s}^{-1} \text{ ppbv}^{-1}$ ,  
360 higher than the average ratio of VOC reactivity to NOx concentration during 2006-  
361 2016 ( $0.24 \text{ s}^{-1} \text{ ppbv}^{-1}$ ). The adverse reduction ratio of VOC to NOx is the main cause of  
362 inefficient reduction in O<sub>3</sub> level in 2008, which is consistent with the study of Chou et  
363 al. (2011).

364 Since 2013, under the implementation of the Action Plan on Air Pollution  
365 Prevention and Control ([http://www.gov.cn/zwggk/2013-09/12/content\\_2486773.htm](http://www.gov.cn/zwggk/2013-09/12/content_2486773.htm)),  
366 more stringent emission control measures were implemented to restrict industrial and  
367 vehicle emission. As a result, there are indications that both VOCs and NO<sub>x</sub> decreased  
368 faster over the 2013 to 2016 period:  $0.81 \text{ s}^{-1} \text{ yr}^{-1}$  ( $16\% \text{ yr}^{-1}$ ,  $r^2 = 0.71$ ) and  $1.94 \text{ ppbv yr}^{-1}$   
369 ( $9.3\% \text{ yr}^{-1}$ ,  $r^2 = 0.78$ ) for VOC reactivity and NO<sub>x</sub>, respectively. This could be the  
370 cause of the decline in O<sub>3</sub> concentrations from 2014 to 2016.

### 371 **3.3 Trend of particulate matter**

372 From 2009 to 2016, PM<sub>2.5</sub> concentrations declined rapidly, achieving the air  
373 quality standard of China ( $35 \mu\text{g}/\text{m}^3$ ) in 2016 (Figure 6). Since 2000, Beijing had  
374 implemented 16 phases' air pollution control measures, mainly including the  
375 controlling of industry, motor vehicle, coal combustion and fugitive dust pollution,  
376 which was effective for the reduction in PM<sub>2.5</sub> (Lang et al., 2017). Especially the  
377 strengthening of the reduction in coal combustion, which was gradually replaced by  
378 natural gas since 2004, favored improved visibility in Beijing (Zhao et al., 2011).

379 As shown in Figure 6, from 2006 to 2016 AOD decreased at a rate of  $9.3\% \text{ yr}^{-1}$ .  
380 The correlation between AOD and PM<sub>2.5</sub> can be determined from the observations of  
381 PM<sub>2.5</sub> and AOD in August during 2009-2016 at the PKUERS site (Figure 7). AOD  
382 and PM<sub>2.5</sub> are linearly correlated with a correlation coefficient of +0.74. This result  
383 indicates that the decrease in PM<sub>2.5</sub> was the primary cause of the reduction in AOD. In  
384 addition to PM<sub>2.5</sub>, relative humidity also has an important effect on AOD. The  
385 decrease in relative humidity during 2006-2016 (Figure 4) would reduce the  
386 hygroscopic growth of aerosol, leading to a weakened extinction effect of particulate  
387 matter on solar radiation (Qu et al., 2015). It is worth noting that although PM<sub>2.5</sub> in  
388 2011 was lower than that in 2010, AOD in 2011 was higher than that in 2010 (Figure  
389 6). For one reason, the relative humidity in 2011 was higher. Additionally, the aerosol  
390 type, atmospheric boundary layer height and the vertical structure of aerosol  
391 distribution also affects the dependence of AOD on PM<sub>2.5</sub> (Zheng et al., 2017),

392 probably contributing to the scatter about the AOD versus PM<sub>2.5</sub> relationship shown in  
393 Figure 7.

394 Monthly mean AE (380/550 nm) in August showed no overall trend during 2006-  
395 2016 (Figure 8). The monthly AE means were between 0.87 and 1.2, suggesting that  
396 the size-distribution of aerosol was generally stable during this period. Monthly mean  
397 SSA (440 nm) in August showed an upward trend of +0.004 yr<sup>-1</sup> (+0.45% yr<sup>-1</sup>, p =  
398 0.001) during 2006-2016 (Figure 8), indicating the proportion of the light-absorbing  
399 component of aerosols (e.g. black carbon) has decreased, due to the stringent and  
400 effective controls on the burning of biomass/biofuel and coal (Ni et al., 2014; Cheng et  
401 al., 2013). This result is consistent with the studies of Lang et al. and Wang et al.,  
402 which indicated that black carbon in China's mega cities has decreased rapidly over  
403 the past decade (Wang et al., 2016b; Lang et al., 2017).

#### 404 3.4 Trend of photolysis frequencies

405 The influence of solar radiation on O<sub>3</sub> photochemistry can be described by  
406 actinic flux (or photolysis frequencies). We chose j(NO<sub>2</sub>) as a representative  
407 photolysis frequency to analyze the trend of actinic flux. Wang et al (2019) studied the  
408 quantitative relationship between j(NO<sub>2</sub>) and AOD at the PKUERS site, and found  
409 that j(NO<sub>2</sub>) and AOD showed a clear nonlinear negative correlation at a given SZA,  
410 with slopes ranging from -1.3 to  $-3.2 \times 10^{-3} \text{ s}^{-1}$  at AOD < 0.7, indicating a significant  
411 extinction effect of AOD on actinic flux near the ground.

412 The j(NO<sub>2</sub>) calculated by the TUV model under clear-sky conditions shows an  
413 upward trend of 3.6% yr<sup>-1</sup> from 2005 to 2016 and agrees well with the 5 years of  
414 observed values from 2011 to 2016 (Figure 6). According to sensitivity analysis of  
415 TUV, the decrease in AOD plays a dominant role in the j(NO<sub>2</sub>) increase, contributing  
416 about 80% of the total. Additionally, the increase in SSA also contributes significantly  
417 to j(NO<sub>2</sub>) increase, contributing about 17%.

418 In addition to aerosol optical properties, the photolysis frequency in the planetary  
419 boundary layer is affected by other factors, including cloud extinction, ground

420 reflection, absorption by gases such as O<sub>3</sub>, and Rayleigh scattering by gases. The  
421 ground reflection is relatively stable for different years in the same city with stable  
422 ground covering. The change in Rayleigh scattering of gases and absorption of NO<sub>2</sub>,  
423 SO<sub>2</sub> and HCHO plays a negligible role in the variation in photolysis frequencies  
424 according to sensitivity analysis of TUV model. This is consistent with the results of  
425 Barnard et al. (Barnard et al., 2004). As shown in Figure 9, the total ozone column  
426 fluctuated between 285-307 DU without a significant overall trend. The magnitude of  
427 total ozone column variation (22 DU) can change j(O<sup>1</sup>D) by about 10%, but plays a  
428 negligible role in changing other photolysis frequencies according to sensitivity  
429 analysis using the TUV model. The cloud optical thickness (COT) for most years was  
430 relatively stable, ranging from 6 to 8, but in 2005, 2012 and 2015 COT was  
431 significantly larger (Figure 9). As there was no significant trend of COT, we surmised  
432 that the light-extinction effect of clouds did not play a key role in determining the  
433 trend of photolysis frequencies.

### 434 3.5 Combined effect of changes in ozone precursors and aerosols on ozone production

435 We investigated the overall effect of the changes in VOCs, NO<sub>x</sub>, photolysis  
436 frequency, and aerosol uptake of HO<sub>2</sub> on ozone production rate using the chemical  
437 box model. [We focus on the period during 2006-2016 due to the lack of NO<sub>x</sub> data in](#)  
438 [2005](#). By testing the response of P(O<sub>3</sub>) as calculated from Equation E1 to the changes  
439 of VOCs and NO<sub>x</sub> concentrations (Figure 10), we concluded that photochemical  
440 environment of the PKUERS site was, on average, in the VOC-limited regime. This  
441 result is consistent with previous studies (Zhang et al., 2014;Chou et al., 2011). Under  
442 this condition, the long-term decrease in VOCs in Beijing has contributed to a  
443 decrease in P(O<sub>3</sub>), while the decrease in NO<sub>x</sub> has tended to increase P(O<sub>3</sub>). As shown  
444 in Figure 11, when the increase in photolysis frequencies and aerosol uptake of HO<sub>2</sub>  
445 were not included in the calculation, the simulated daytime average P(O<sub>3</sub>) decreased  
446 slightly at a rate of 1.1% yr<sup>-1</sup>. This indicates that the ratio of the rates of decrease of  
447 VOCs and NO<sub>x</sub> (about 1.1) is nearly inefficient in reducing ozone production in

448 Beijing. However, when the increase in photolysis frequencies was included in the  
449 model calculation, the calculated daytime average  $P(O_3)$  showed an increasing trend  
450 of  $2.2\% \text{ yr}^{-1}$ . This result indicates that the increase in photolysis frequencies more  
451 than compensated for the downward trend of  $O_3$  production driven by decreased  
452 VOCs and  $NO_x$ , leading to increasing  $O_3$  production through the decade. The  
453 photochemical box model calculations indicate that the increase in photolysis  
454 frequencies has two major impacts on  $P(O_3)$  - an increase in primary production of  
455 OH through accelerated photolysis of  $O_3$ , HONO, HCHO and other carbonyl  
456 compounds, and an accelerated radical recycling of OH as VOCs are oxidized. As  
457 particulate matter has decreased and photolysis frequencies correspondingly have  
458 increased, a more rapidly decreasing rate of the VOC to  $NO_x$  ratio is required to  
459 achieve a significant reduction in  $O_3$  in the future.

460 The simulated  $P(O_3)$  in the afternoon hour (12:00-15:00) when ozone production  
461 is active and HOx levels are high increased at a rate of  $1.3\% \text{ yr}^{-1}$ , which is lower than  
462 the increasing rate of daytime average  $P(O_3)$  ( $2.2\% \text{ yr}^{-1}$ ) (Figure S2). Hollaway et al.  
463 (2019) show that the impacts of aerosols on the summertime photolysis of  $NO_2$  and  
464 ozone at surface in Beijing are important before 11:00 am and after 3:00 pm but very  
465 limited in afternoon hours due to smaller SZA and lower light absorption of aerosol  
466 (i.e. higher SSA) in the afternoon. However, the diurnal variation of simulated  $P(O_3)$   
467 in this study indicates that the influence of aerosols on  $P(O_3)$  is still significant in the  
468 afternoon, leading to average  $P(O_3)$  decreased by  $\sim 17\%$  (Figure S3), which is slightly  
469 lower than the mean daytime decrease (25%). This is because the average AOD in the  
470 afternoon (1.4) is significantly higher than that before 11:00 am (0.94) and after 3:00  
471 pm (1.1) despite the smaller SZA and higher SSA.

472

473 When we include heterogeneous uptake of  $HO_2$  in the model, the calculated  
474  $P(O_3)$  increases at a faster rate of  $2.9\% \text{ yr}^{-1}$  due to the overall reduced aerosol surface  
475 concentration ( $S_a$ ), which reduces heterogeneous uptake of  $HO_2$  (Figure 11). This  
476 result indicates that the effect of heterogeneous uptake of  $HO_2$  contributed roughly  
477  $0.7\% \text{ yr}^{-1}$  to the  $P(O_3)$  increase. Hence, our result indicates that the increase in

478 photolysis rates due to PM decrease plays a more important role than the decrease in  
479 heterogeneous uptake of HO<sub>2</sub> by aerosols in accelerating ozone production in Beijing.  
480 Previous measurements indicate that the uptake coefficient varies widely from 0.003  
481 to 0.5 with a strong dependence on the aerosol concentration of transition metal ions  
482 such as Cu(II) (Zou et al., 2019;Taketani et al., 2008;Lakey et al., 2015;Matthews et  
483 al., 2014;Lakey et al., 2016). This strong dependence on aerosol composition implies  
484 that a single assumed value for  $\gamma_{\text{HO}_2} = 0.2$  has large uncertainty.  $\gamma_{\text{HO}_2} = 0.2$  used in our  
485 simulation is likely an overestimate of the effect of heterogeneous uptake of HO<sub>2</sub> on  
486 ozone production rate at PKUERS site.

487 A few heterogeneous chemical reactions of nitrogen oxides are thought to be  
488 potential influential factors of ozone production. For example, the heterogeneous  
489 uptake of NO<sub>2</sub> to produce HNO<sub>3</sub> and HONO, and the heterogeneous uptake of NO<sub>3</sub>  
490 and N<sub>2</sub>O<sub>5</sub> to produce HNO<sub>3</sub>. Our simulation indicates that the reduced heterogeneous  
491 uptake of NO<sub>x</sub> caused P(O<sub>3</sub>) to increase by only ~2.2 % during 2006-2016. Li et al.  
492 (2019b) also reported that the effect of heterogeneous uptake of nitrogen oxides on  
493 ozone is very small under VOC-limited and summertime conditions in North China  
494 Plain. Our simulated result in summertime Beijing, where VOC-limited  
495 photochemistry dominates, is consistent with the result of Li et al. (2019b).

496 In summertime, PM in the Beijing urban area is mainly formed by the secondary  
497 conversion of gaseous precursors (Han et al., 2015;Guo et al., 2014), indicating that  
498 VOCs and NO<sub>x</sub> are not only the precursors of ozone, but also the main precursors of  
499 PM in this urban area. In addition, observations in Beijing have shown that the  
500 secondary components of PM, including secondary organic matter, ammonium sulfate  
501 and ammonium nitrate, dominate the light extinction of PM (Han et al., 2014;Han et al.,  
502 2017;Wang et al., 2015b). As a result, reductions of VOCs and NO<sub>x</sub> are expected to  
503 lead to a decrease in secondary PM formation, and thus to further enhancement in solar  
504 radiation (or actinic flux). Therefore, in order to reduce ozone effectively, the  
505 contribution of VOCs and NO<sub>x</sub> to secondary PM formation and their effect on solar  
506 radiation must be comprehensively considered. However, the summertime formation of  
507 PM is quite complex; the conversion efficiency of gaseous precursors to aerosols and

508 the resulting influence on ozone production is a research area that requires further study.

### 509 **3.6 Additional considerations**

510 One limitation of this study is that the photochemical box model is constrained  
511 by surface observations, and hence may not accurately represent some aspects of the  
512 photochemistry through the full depth of the planetary boundary layer over Beijing.  
513 Here we briefly consider several of these aspects: (1) The treatment of ozone and  
514 VOC and NO<sub>x</sub> precursor concentrations likely are accurately represented, because  
515 rapid daytime vertical mixing ensures that there is only a small vertical gradient in the  
516 concentrations of these relatively long-lived species. (2) In daytime, the HONO  
517 lifetime is so short that it may be largely confined to near the surface, where it has  
518 surface sources (heterogeneous reaction of H<sub>2</sub>O and NO<sub>2</sub> and emissions on surfaces).  
519 Therefore, the estimated HONO based on near-surface NO<sub>2</sub> concentrations may  
520 overestimate average boundary layer HONO concentrations; however, in this study  
521 the influence of HONO on the calculation is relatively small, so this is not a large  
522 source of error. (3) The model is constrained by surface measurements of photolysis  
523 frequencies, but these surface measurements do not accurately quantify the actinic  
524 flux throughout the boundary layer. Figure 12 presents the vertical profiles of  $j(\text{NO}_2)$   
525 simulated by the TUV model for aerosol properties representative of Beijing. A thick  
526 layer of aerosol effectively reduces radiation at the bottom of the layer, but not at the  
527 top, where radiation may be enhanced due to upward scattering from the aerosol  
528 below (Dickerson et al., 1997; Jacobson, 1998). Overall, vertical average  $j(\text{NO}_2)$   
529 increased by 32% from 2006 to 2016, which is comparable to the surface increase  
530 (36%). These simulations indicate that the increased trend of  $j(\text{NO}_2)$  derived from  
531 surface observations do approximate the trend through the entire boundary layer.  
532 However, there is a shift in the vertical profile of  $j(\text{NO}_2)$  that is important. The  
533 crossing point between  $j(\text{NO}_2)$  profile of 2006 and zero AOD profile is below PBL,  
534 while in 2016 the  $j(\text{NO}_2)$  profile crosses the zero AOD profile within the PBL. This  
535 means that as the AOD is reduced further, changes in the vertical average  $j(\text{NO}_2)$  will

536 be limited, since increases in  $j(\text{NO}_2)$  near the top of the PBL will compensate for  
537 decreases near the surface. Additionally, this also denotes that the role of  $\text{PM}_{2.5}$  may  
538 be more important under condition like 2006, but will be limited under condition like  
539 2016 when there is offsetting effect for PBL ozone by vertical mixing caused by  
540 larger ozone vertical gradient (Gao et al., 2020).

541 Quantitative studies suggested that, the impact of aerosols via affecting  
542 photolysis rates led to surface ozone concentrations decreasing by 2%–17%  
543 (Jacobson, 1998;Li et al., 2011a;Li et al., 2011b;Wang et al., 2016a). However, these  
544 studies also showed that ozone net production decreased more (15 ~ 30%) (Cai,  
545 2013;Wang et al., 2019;Castro et al., 2001), which did not match the magnitude of the  
546 reduction in surface ozone concentrations. The difference between the two reductions  
547 in ozone production and surface ozone concentration indicates that, in addition to  
548 ozone photochemistry, there must be other ozone related physical processes  
549 influenced by the reduction in photolysis rate induced by aerosols. Model simulation  
550 indicates that aerosols lead to high concentrations of ozone aloft being entrained by  
551 turbulence from the top of the planetary boundary layer (PBL) to the surface by  
552 altering photolysis rate and partly counteracting the reduction in surface ozone  
553 photochemical production induced by aerosols. In addition, the impact of aerosols on  
554 ozone from local and adjacent regions was more significant than that from long-  
555 distance regions (Gao et al., 2020). Therefore, the accurate quantification of the  
556 effects of vertical mixing and long-distance transport on surface ozone concentration  
557 plays a critical role in the impact of aerosols on surface ozone, which needs further  
558 study in the future.

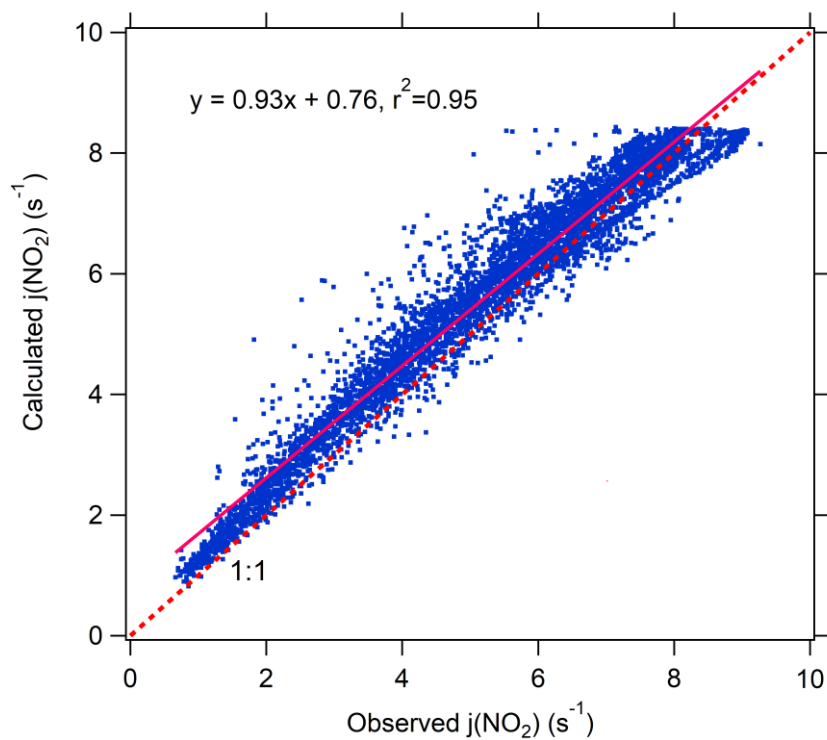
## 559 **4 Conclusion**

560 During the past decade, China has devoted very substantial resources to  
561 improving the environment. These efforts have improved atmospheric particulate  
562 matter loading, but ambient ozone levels have continued to increase. Based on the

563 long-term measurements at a representative site in Beijing, we explored the factors  
564 driving the increase in ozone production. Consistent with the implementation of  
565 stringent emission control measures, concentrations of PM<sub>2.5</sub> and ozone precursors  
566 (VOCs and NO<sub>x</sub>) decreased rapidly, but in contrast O<sub>3</sub> and O<sub>x</sub> increased. This  
567 investigation finds that the primary cause of the O<sub>3</sub> increase is that decreasing PM  
568 concentrations led to an increase in actinic flux, which in turn increased the  
569 photochemical production of ozone. This result indicates that the influence of aerosol  
570 on ozone production is important for determining the full manifold of atmospheric  
571 effects that result from reducing the emissions of the O<sub>3</sub> and PM precursors.

## 572 **ACKNOWLEDGEMENTS**

573 This work was supported by the Major Program of the National Natural Science  
574 Foundation of China [Grant number 91644222]. We thank Hongbin Chen and  
575 Philippe Goloub for data management of AOD and other aerosol optical properties on  
576 AERONET.

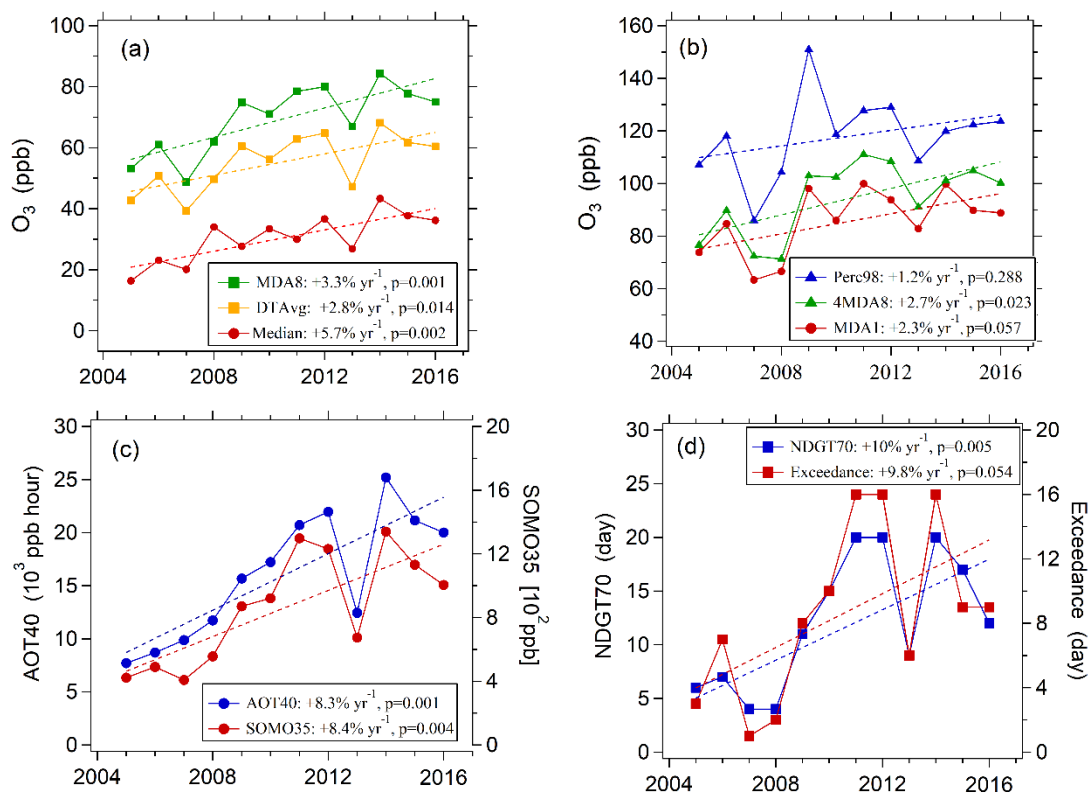


577

578 Figure 1. Correlation between Observed and calculated  $j(\text{NO}_2)$  by TUV model in

579 Beijing in summer time during 2012 - 2015.

580



582

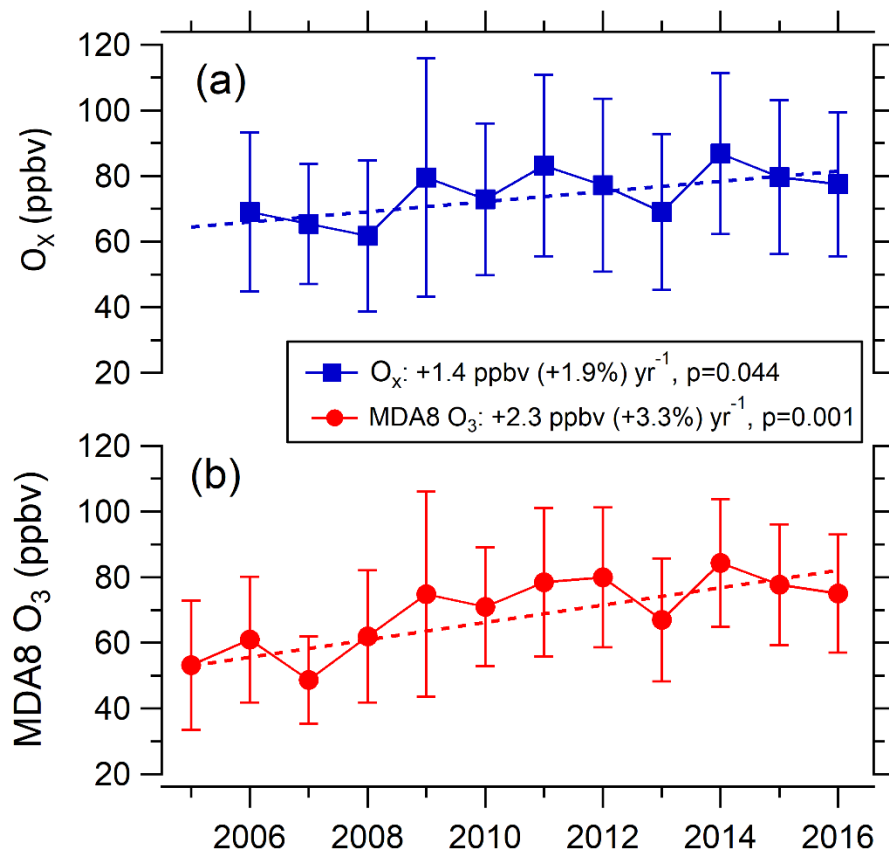
583 Figure 2. Variations in multiple O<sub>3</sub> metrics at the PKUERS site in Beijing in August

584 between 2005 and 2016.

585

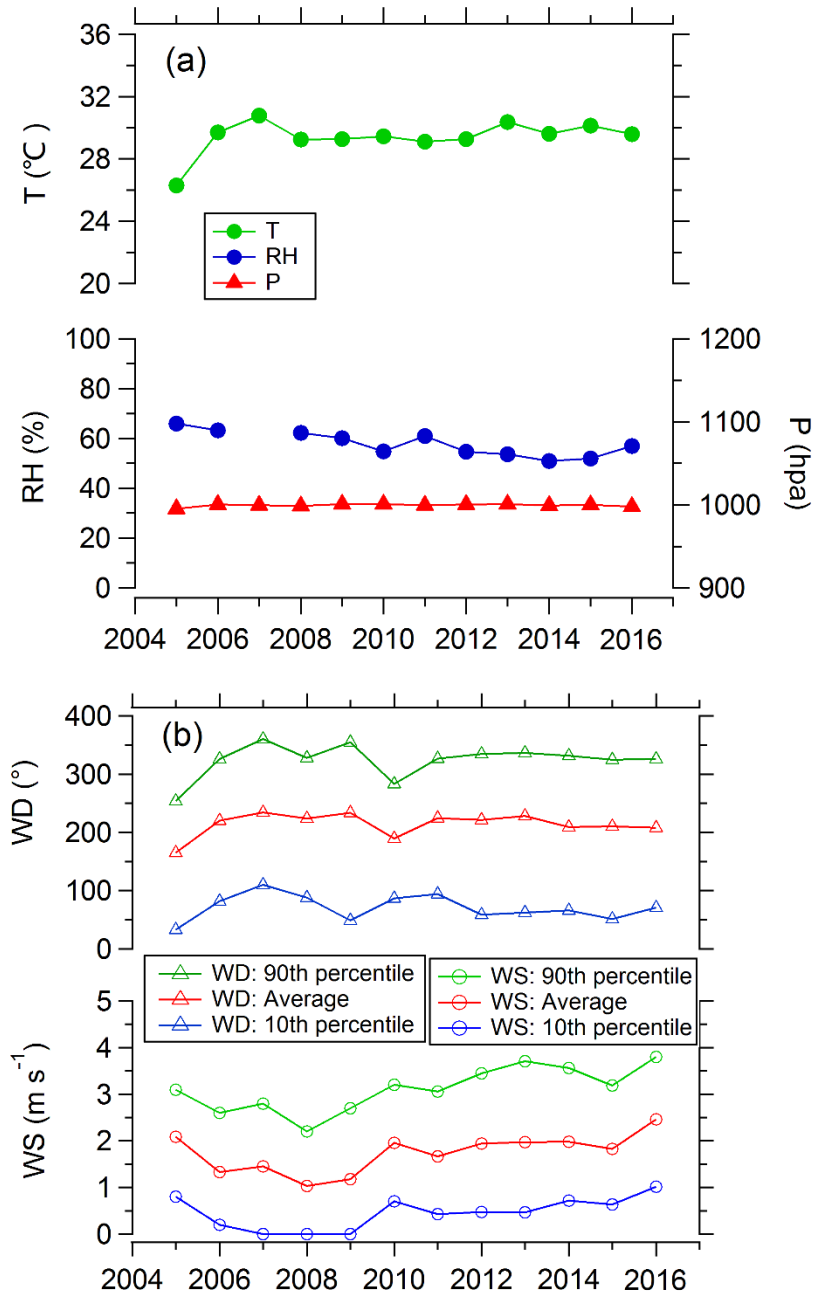
586

587  
588



589  
590  
591  
592

Figure 3. Variations in average MDA8 O<sub>3</sub> and daytime (7:00-19:00) average Ox in Beijing, August between 2005 and 2016.



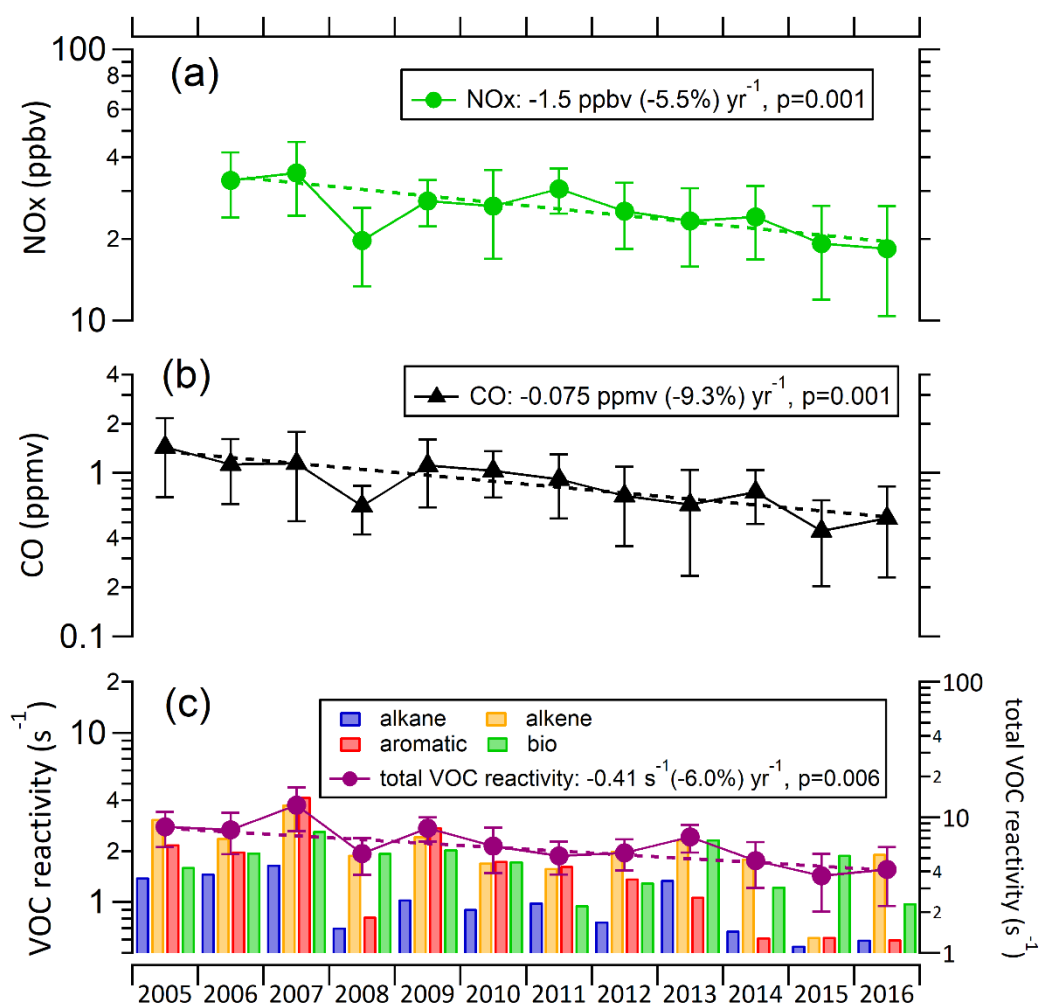
593

594 Figure 4. Variations in daytime (7:00-19:00) averages of meteorological conditions  
 595 including temperature (T), relative humidity (RH), wind direction (WD) and wind  
 596 speed (WS) in Beijing, August during 2005 - 2016.

597

598

599



600

601 Figure 5. Variations in arithmetic mean MDA8 O<sub>3</sub>, arithmetic mean of daytime (7:00-

602 19:00) Ox and geometric mean of daytime NO<sub>x</sub>, CO and VOCs reactivity in Beijing,

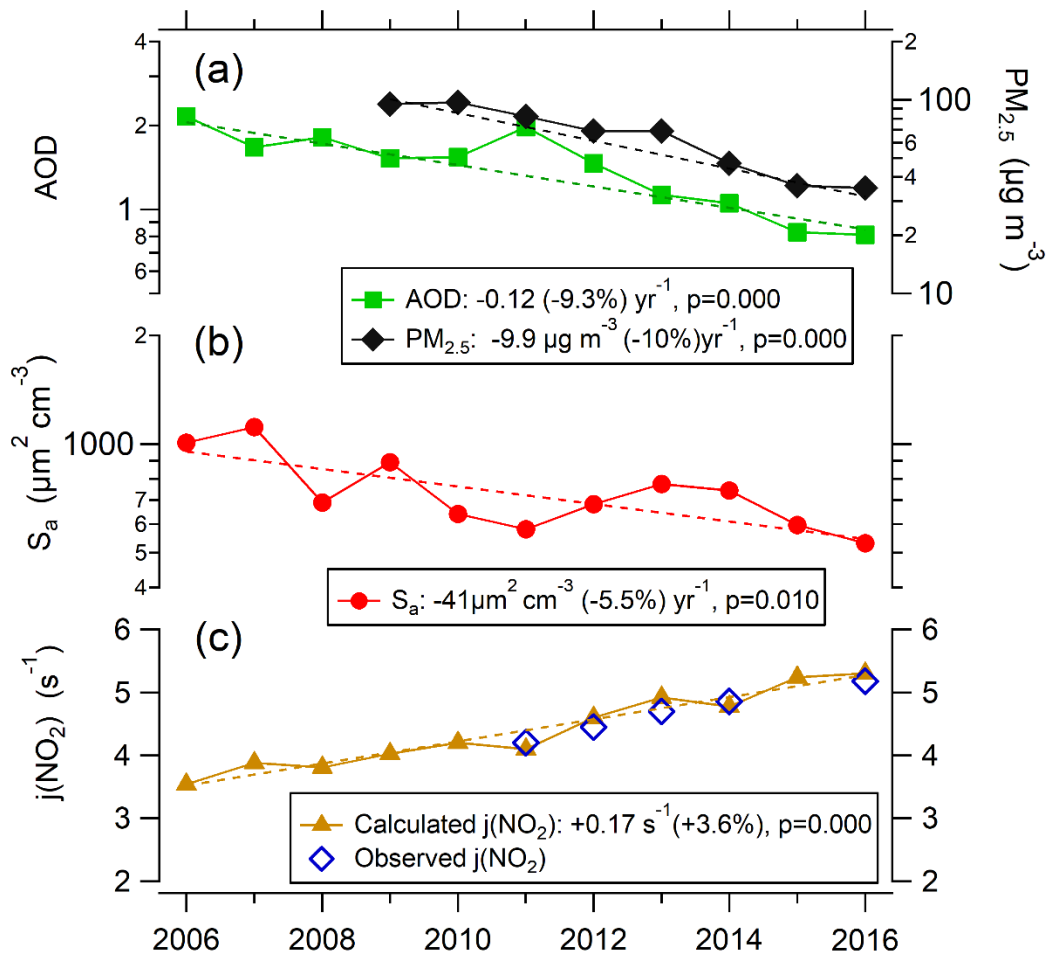
603 August between 2005 and 2016. VOCs reactivity is depicted by reactivity of each

604 species (left axis) and total VOC reactivity (right axis). On the y-axes, a linear scale is

605 used for O<sub>3</sub> and Ox, and a log-scale is used for the precursor concentrations (NO<sub>x</sub>,

606 CO and VOCs).

607

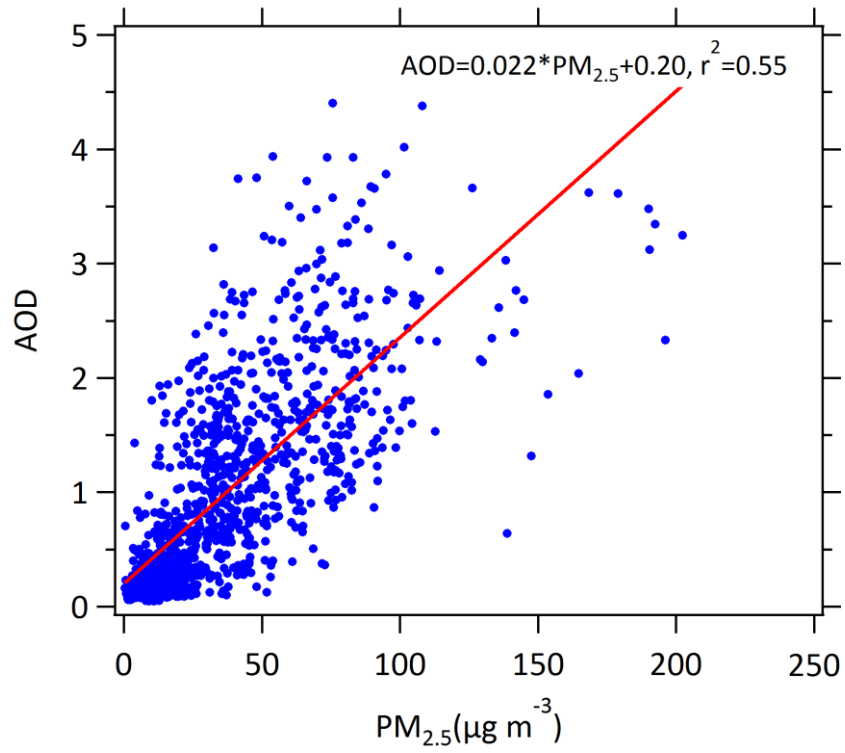


608

609 Figure 6. Variations in daytime (7:00-19:00) averages of AOD (380 nm), PM<sub>2.5</sub>, S<sub>a</sub>,  
 610 j(NO<sub>2</sub>) Calculated j(NO<sub>2</sub>) by TUV in Beijing, August between 2006 and 2016. AOD  
 611 and j(NO<sub>2</sub>) are both corresponding to cloudless weather. On the y-axes, a log-scale is  
 612 used for PM<sub>2.5</sub>, AOD and S<sub>a</sub> and a linear scale is used for j(NO<sub>2</sub>).

613

614

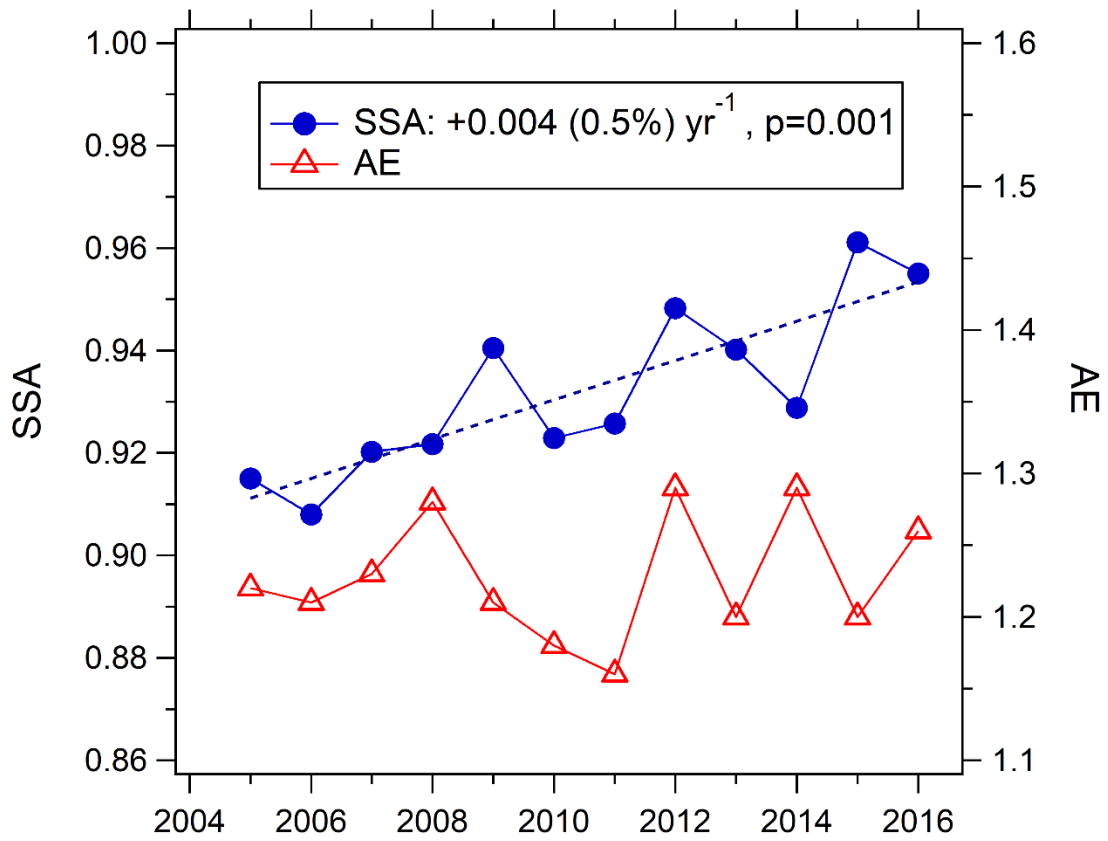


615

616 Figure 7. Correlation between AOD and PM<sub>2.5</sub> in Beijing, summertime during 2009 -

617 2016.

618



619

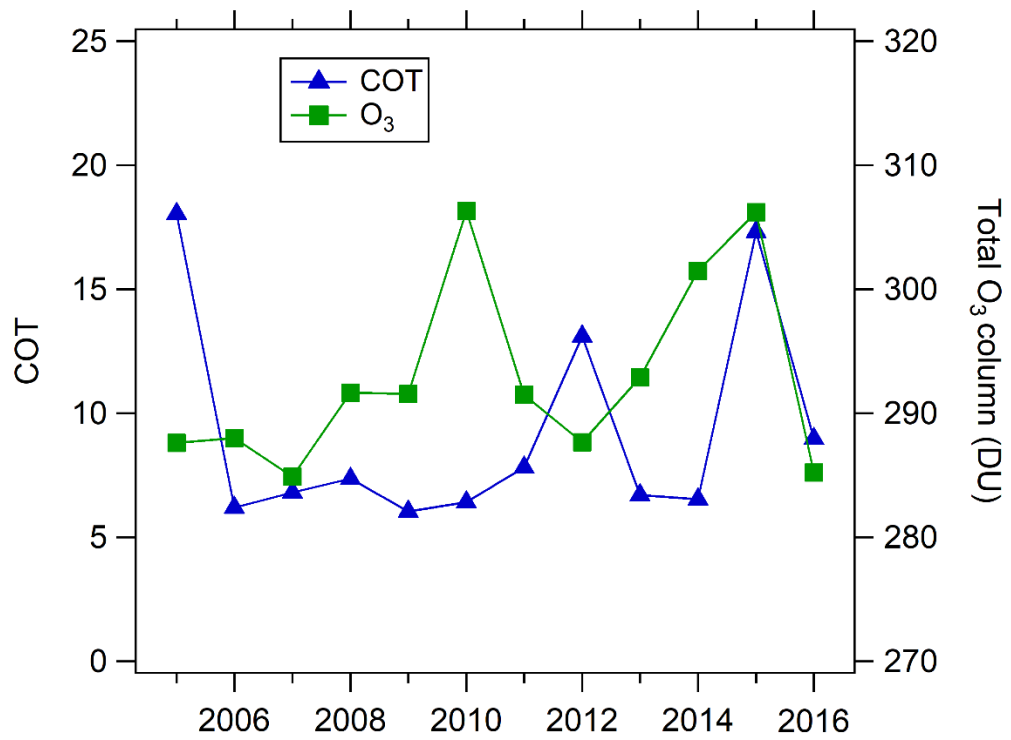
620 Figure 8. Variation in monthly mean single scattering albedo (SSA) and Ångström

621 exponent (AE) in Beijing for the month of August during 2005 - 2016.

622

623

624



625

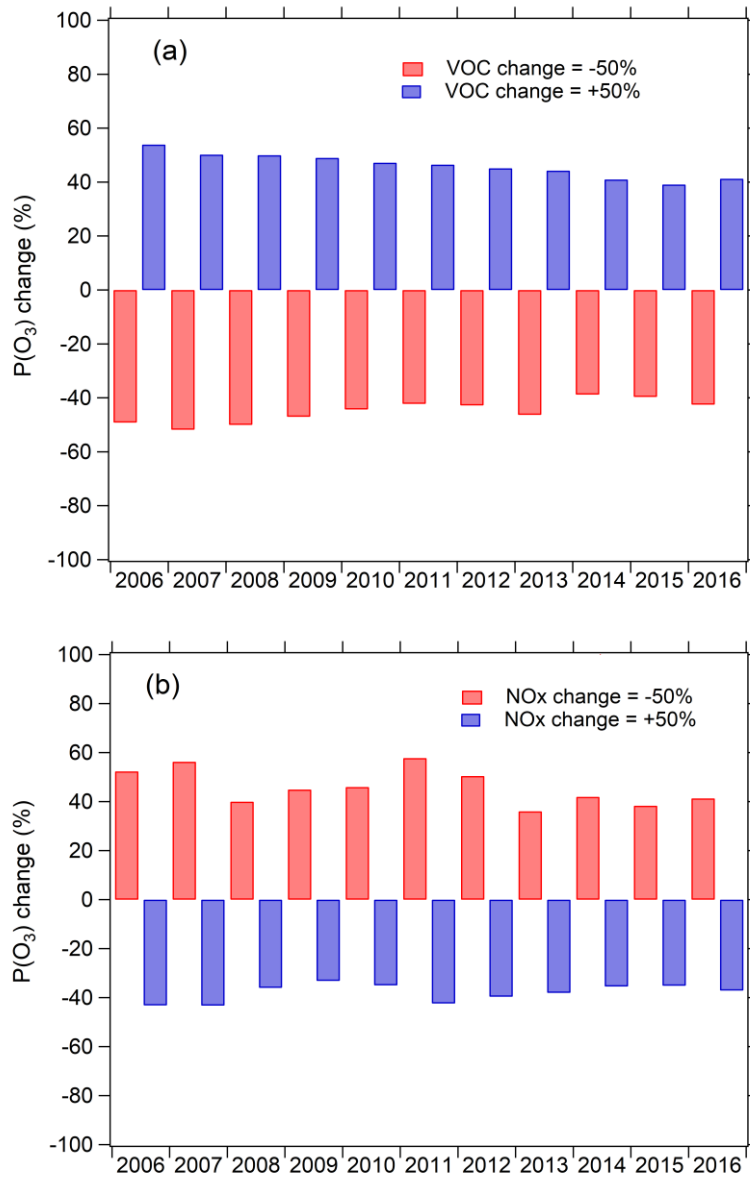
626 Figure 9. Variations in mean total ozone column and cloud optical thickness (COT) in

627 Beijing for the month of August during 2005 - 2016.

628

629

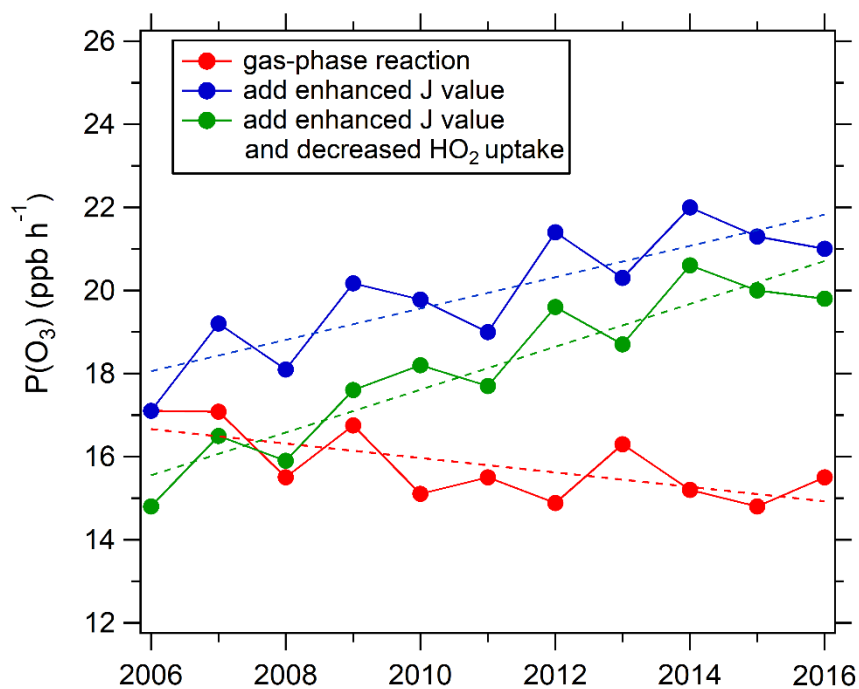
630



631

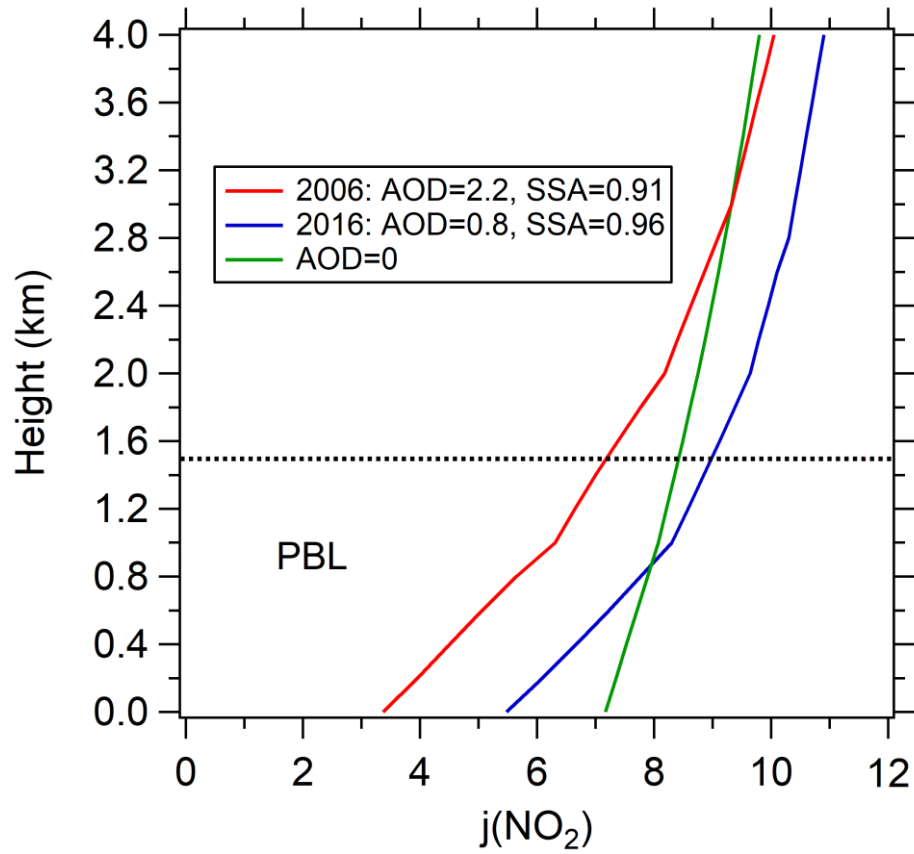
632 Figure 10. Sensitivity of monthly daytime mean  $P(O_3)$  to VOCs and  $NO_x$  simulated  
 633 by box model during 2006 - 2016. VOCs and  $NO_x$  is increased by 50% or decreased  
 634 by 50% to test the fractional change of monthly daytime mean  $P(O_3)$ .

635



637

638 Figure 11. Trend of monthly daytime mean  $P(O_3)$  simulated by the chemical box  
 639 model. Red dots: Only the gas-phase reactions are considered in the box model  
 640 constrained by observed photolysis frequencies from 2006 for all eleven years. Blue  
 641 dots: the box model as above, but constrained by the photolysis frequencies derived  
 642 for each year. Green dots: the box model constrained by the photolysis frequencies  
 643 derived for each year with the changing aerosol uptake of  $HO_2$  also considered.  
 644



645

646 Figure 12. Vertical profiles of  $j(\text{NO}_2)$  simulated by the TUV model in Beijing. Three  
 647 scenarios are simulated: The model parameters are: (1) AOD=2.2, SSA=0.91 in August  
 648 2006; (2) AOD=0.8, SSA=0.96 in August 2016; (3) AOD=0. The daytime average  
 649 SZA=53° is used for all simulations. Dotted line represent the top of boundary layer.

650

651

652 Table 1. Instruments deployed in the measurement undertaken in August during 2005 -  
 653 2016 and used for data analysis.

Parameters	Measurement technique	Time resolution	Detection limit	Accuracy
Photolysis frequencies	Spectroradiometer	10 s	/	± 10%
O <sub>3</sub>	UV photometry	60 s	0.5 ppbv	± 5%
NO	Chemiluminescence	60 s	60 pptv	± 20%
NO <sub>2</sub>	Chemiluminescence	60 s	300 pptv	± 20%
CO	IR photometry	60 s	4 ppb	± 5%
SO <sub>2</sub>	Pulsed UV fluorescence	60 s	0.1 ppbv	± 5%
HCHO	Hantzsch fluorimetry	60 s	25 pptv	± 5%
C2-C10VOCs	GC-FID/MS	1 h	20-300 pptv	± 15~20%
PM <sub>2.5</sub>	TH-2000	60s	1µg m <sup>-3</sup>	± 5%
S <sub>a</sub>	SMPS	60s	/	±3%
AOD, SSA, AE	CIMEL Sun photometer	5min	0.01	±5%

654

655

656

Table 2. p value of temporal trends for different parameters.

Parameter	Period	r <sup>2</sup>	p value	P value <0.01?	P value <0.05?
median	2005-2016	0.63	0.002	yes	yes
perc98	2005-2016	0.11	0.288	no	no
DTAvg	2005-2016	0.47	0.014	no	yes
MDA1	2005-2016	0.32	0.057	no	no
MDA8	2005-2016	0.66	0.001	yes	yes
4MDA8	2005-2016	0.42	0.023	no	yes
AOT40	2005-2016	0.67	0.001	yes	yes
NDGT70	2005-2016	0.56	0.005	yes	yes
SOMO35	2005-2016	0.57	0.004	yes	yes
exceedance	2005-2016	0.32	0.054	no	no
Ox	2005-2016	0.38	0.044	no	yes
CO	2005-2016	0.87	0.001	yes	yes
VOC reactivity	2005-2016	0.52	0.006	yes	yes
NO <sub>x</sub>	2006-2016	0.81	0.001	yes	yes
Calculated j(NO <sub>2</sub> )	2006-2016	0.94	0.000	yes	yes
AOD (380 nm)	2006-2016	0.78	0.000	yes	yes
PM <sub>2.5</sub>	2009-2016	0.93	0.000	yes	yes
Sa	2006-2016	0.51	0.010	yes	yes
SSA	2005-2016	0.70	0.001	yes	yes
AE	2005-2016	0.03	0.593	no	no
COT	2005-2016	0.003	0.875	no	no
Total O <sub>3</sub> column	2005-2016	0.15	0.215	no	no

657

658

659

660

661

662

663

664

665

666

667

668

669 Table 3. Description of Ozone Metrics used in this study.

categories	metric	definition
general level	median (ppb)	50th percentile of hourly concentrations
	MDA8 (ppb)	daily maximum 8 h average; the mean MDA8 O <sub>3</sub> in August of each year is used in this study.
	DTAvg (ppb)	daytime average ozone is the average of hourly ozone concentrations for the 12 h period from 07:00 to 19:00 local time
extreme level	MDA1 (ppb)	daily maximum 1 h average; the mean MDA1 O <sub>3</sub> in August of each year is used in this study.
	Perc98 (ppb)	98th percentile of hourly concentrations
	4MDA8 (ppb)	4th highest MDA8
ozone exposure	AOT40 (ppb h)	cumulative hourly ozone concentrations of >40 ppb
	SOMO35 (ppb day)	sum of positive differences between MDA8 and a cutoff concentration of 35 ppb
Exceedance days	NDGT70 (day)	total number of days with MDA8 values of >70 ppb
	Exceedance (day)	number of days with the ozone concentration exceeding the Chinese grade II national air quality standard, defined as MDA8 > 160 μg m <sup>-3</sup>

670

671

672 **Reference**

- 673 Atkinson, R.: Atmospheric chemistry of VOCs and NO<sub>x</sub>, *Atmos. Environ.*, **34**, 2063-2101, 2000.
- 674 Barnard, J. C., Chapman, E. G., Fast, J. D., Schmelzer, J. R., Slusser, J. R., and Shetter, R. E.: An  
675 evaluation of the FAST-J photolysis algorithm for predicting nitrogen dioxide photolysis rates  
676 under clear and cloudy sky conditions, *Atmos. Environ.*, **38**, 3393-3403,  
677 <https://doi.org/10.1016/j.atmosenv.2004.03.034>, 2004.
- 678 Bohn, B., Corlett, G. K., Gillmann, M., Sanghavi, S., Stange, G., Tensing, E., Vrekoussis, M., Bloss, W.  
679 J., Clapp, L. J., Kortner, M., Dorn, H. P., Monks, P. S., Platt, U., Plass-Dulmer, C., Mihalopoulos, N.,  
680 Heard, D. E., Clemitshaw, K. C., Meixner, F. X., Prevot, A. S. H., and Schmitt, R.: Photolysis frequency  
681 measurement techniques: results of a comparison within the ACCENT project, *Atmospheric*  
682 *Chemistry and Physics*, **8**, 5373-5391, 10.5194/acp-8-5373-2008, 2008.
- 683 Cai, Y. F., Wang, T. J., and Xie, M.: Impacts of atmospheric particles on surface ozone in Nanjing  
684 (In Chinese), *Climatic Environment Research*, **18**, 251-260, 10.5194/acp-8-6155-2008, 2013.
- 685 Castro, T., Madronich, S., Rivale, S., Muhlia, A., and Mar, B.: The influence of aerosols on  
686 photochemical smog in Mexico City, *Atmos. Environ.*, **35**, 1765-1772,  
687 [https://doi.org/10.1016/S1352-2310\(00\)00449-0](https://doi.org/10.1016/S1352-2310(00)00449-0), 2001.
- 688 Cheng, Y., Engling, G., He, K. B., Duan, F. K., Ma, Y. L., Du, Z. Y., Liu, J. M., Zheng, M., and Weber, R.  
689 J.: Biomass burning contribution to Beijing aerosol, *Atmos. Chem. Phys.*, **13**, 7765-7781,  
690 10.5194/acp-13-7765-2013, 2013.
- 691 Chou, C. C. K., Tsai, C. Y., Chang, C. C., Lin, P. H., Liu, S. C., and Zhu, T.: Photochemical production  
692 of ozone in Beijing during the 2008 Olympic Games, *Atmos. Chem. Phys.*, **11**, 9825-9837,  
693 10.5194/acp-11-9825-2011, 2011.
- 694 de Miranda, R. M., Andrade, M. D., and Fattori, A. P.: Preliminary studies of the effect of aerosols  
695 on nitrogen dioxide photolysis rates in the city of Sao Paulo, Brazil, *Atmospheric Research*, **75**,  
696 135-148, 10.1016/j.atmosres.2004.12.004, 2005.
- 697 Dickerson, R. R., Kondragunta, S., Stenchikov, G., Civerolo, K. L., Doddridge, B. G., and Holben, B.  
698 N.: The Impact of Aerosols on Solar Ultraviolet Radiation and Photochemical Smog, *Science*, **278**,  
699 827-830, 10.1126/science.278.5339.827, 1997.
- 700 Dubovik, O., and King, M. D.: A flexible inversion algorithm for retrieval of aerosol optical properties  
701 from Sun and sky radiance measurements, *Journal of Geophysical Research-Atmospheres*, **105**,  
702 20673-20696, 10.1029/2000jd900282, 2000.
- 703 Fiore, A. M., Dentener, F. J., Wild, O., Cuvelier, C., Schultz, M. G., Hess, P., Textor, C., Schulz, M.,  
704 Doherty, R. M., Horowitz, L. W., MacKenzie, I. A., Sanderson, M. G., Shindell, D. T., Stevenson, D. S.,  
705 Szopa, S., Van Dingenen, R., Zeng, G., Atherton, C., Bergmann, D., Bey, I., Carmichael, G., Collins,  
706 W. J., Duncan, B. N., Faluvegi, G., Folberth, G., Gauss, M., Gong, S., Hauglustaine, D., Holloway, T.,  
707 Isaksen, I. S. A., Jacob, D. J., Jonson, J. E., Kaminski, J. W., Keating, T. J., Lupu, A., Marmor, E.,  
708 Montanaro, V., Park, R. J., Pitari, G., Pringle, K. J., Pyle, J. A., Schroeder, S., Vivanco, M. G., Wind, P.,  
709 Wojcik, G., Wu, S., and Zuber, A.: Multimodel estimates of intercontinental source-receptor  
710 relationships for ozone pollution, *Journal of Geophysical Research-Atmospheres*, **114**, 21,  
711 10.1029/2008jd010816, 2009.
- 712 Fotiadis, A., Hatzianastassiou, N., Drakakis, E., Matsoukas, C., Pavlakis, K. G., Hatzidimitriou, D.,  
713 Gerasopoulos, E., Mihalopoulos, N., and Vardavas, I.: Aerosol physical and optical properties in the

714 Eastern Mediterranean Basin, Crete, from Aerosol Robotic Network data, *Atmospheric Chemistry*  
715 *and Physics*, 6, 5399-5413, 10.5194/acp-6-5399-2006, 2006.

716 Gao, J., Li, Y., Zhu, B., Hu, B., Wang, L., and Bao, F.: What have we missed when studying the impact  
717 of aerosols on surface ozone via changing photolysis rates?, *Atmos. Chem. Phys. Discuss.*, 2020,  
718 1-28, 10.5194/acp-2020-140, 2020.

719 Gao, W., Tie, X. X., Xu, J. M., Huang, R. J., Mao, X. Q., Zhou, G. Q., and Chang, L. Y.: Long-term  
720 trend of O<sub>3</sub> in a mega City (Shanghai), China: Characteristics, causes, and interactions with  
721 precursors, *Science of the Total Environment*, 603, 425-433, 10.1016/j.scitotenv.2017.06.099, 2017.

722 Gerasopoulos, E., Kazadzis, S., Vrekoussis, M., Kouvarakis, G., Liakakou, E., Kouremeti, N.,  
723 Giannadaki, D., Kanakidou, M., Bohn, B., and Mihalopoulos, N.: Factors affecting O<sub>3</sub> and NO<sub>2</sub>  
724 photolysis frequencies measured in the eastern Mediterranean during the five-year period 2002-  
725 2006, *J. Geophys. Res.-Atmos.*, 117, 14, 10.1029/2012jd017622, 2012.

726 Goliff, W. S., Stockwell, W. R., and Lawson, C. V.: The regional atmospheric chemistry mechanism,  
727 version 2, *Atmospheric Environment*, 68, 174-185, 10.1016/j.atmosenv.2012.11.038, 2013.

728 Guo, S., Hu, M., Zamora, M. L., Peng, J., Shang, D., Zheng, J., Du, Z., Wu, Z., Shao, M., Zeng, L.,  
729 Molina, M. J., and Zhang, R.: Elucidating severe urban haze formation in China, *Proceedings of the*  
730 *National Academy of Sciences*, 111, 17373-17378, 10.1073/pnas.1419604111, 2014.

731 Han, T. T., Liu, X. G., Zhang, Y. H., Qu, Y., Gu, J. W., Ma, Q., Lu, K. D., Tian, H. Z., Chen, J., Zeng, L.  
732 M., Hu, M., and Zhu, T.: Characteristics of Aerosol Optical Properties and Their Chemical  
733 Apportionments during CAREBeijing 2006, *Aerosol Air Qual. Res.*, 14, 1431-1442,  
734 10.4209/aaqr.2013.06.0203, 2014.

735 Han, T. T., Liu, X. G., Zhang, Y. H., Qu, Y., Zeng, L. M., Hu, M., and Zhu, T.: Role of secondary aerosols  
736 in haze formation in summer in the Megacity Beijing, *Journal of Environmental Sciences*, 31, 51-  
737 60, 10.1016/j.jes.2014.08.026, 2015.

738 Han, T. T., Xu, W. Q., Li, J., Freedman, A., Zhao, J., Wang, Q. Q., Chen, C., Zhang, Y. J., Wang, Z. F.,  
739 Fu, P. Q., Liu, X. G., and Sun, Y. L.: Aerosol optical properties measurements by a CAPS single  
740 scattering albedo monitor: Comparisons between summer and winter in Beijing, China, *Journal of*  
741 *Geophysical Research-Atmospheres*, 122, 2513-2526, 10.1002/2016jd025762, 2017.

742 Hendrick, F., Muller, J. F., Clemer, K., Wang, P., De Maziere, M., Fayt, C., Gielen, C., Hermans, C., Ma,  
743 J. Z., Pinardi, G., Stavrou, T., Vlemmix, T., and Van Roozendaal, M.: Four years of ground-based  
744 MAX-DOAS observations of HONO and NO<sub>2</sub> in the Beijing area, *Atmospheric Chemistry and*  
745 *Physics*, 14, 765-781, 10.5194/acp-14-765-2014, 2014.

746 Hollaway, M., Wild, O., Yang, T., Sun, Y., Xu, W., Xie, C., Whalley, L., Slater, E., Heard, D., and Liu, D.:  
747 Photochemical impacts of haze pollution in an urban environment, *Atmospheric Chemistry and*  
748 *Physics*, 19, 9699-9714, 2019.

749 Hu, B., Zhao, X., Liu, H., Liu, Z., Song, T., Wang, Y., Tang, L., Xia, X., Tang, G., Ji, D., Wen, T., Wang,  
750 L., Sun, Y., and Xin, J.: Quantification of the impact of aerosol on broadband solar radiation in  
751 North China, *Scientific Reports*, 7, 44851, 10.1038/srep44851, 2017.

752 Jacob, D. J.: Heterogeneous chemistry and tropospheric ozone, *Atmos. Environ.*, 34, 2131-2159,  
753 2000.

754 Jacobson, M. Z.: Studying the effects of aerosols on vertical photolysis rate coefficient and  
755 temperature profiles over an urban airshed, *Journal of Geophysical Research: Atmospheres*, 103,  
756 10593-10604, 10.1029/98jd00287, 1998.

757 Jinfeng, Keding, Liuju, Zhong, Yubo, Duohong, Chen, Huang, Yuanhang, and Zhang: Fast

758 increasing of surface ozone concentrations in Pearl River Delta characterized by a regional air  
759 quality monitoring network during 2006–2011, *Journal of Environmental Sciences*, 26, 23–36, 2014.

760 Lakey, P. S. J., George, I. J., Whalley, L. K., Baeza-Romero, M. T., and Heard, D. E.: Measurements  
761 of the HO<sub>2</sub> Uptake Coefficients onto Single Component Organic Aerosols, *Environ. Sci. Technol.*,  
762 49, 4878–4885, 10.1021/acs.est.5b00948, 2015.

763 Lakey, P. S. J., George, I. J., Baeza-Romero, M. T., Whalley, L. K., and Heard, D. E.: Organics  
764 Substantially Reduce HO<sub>2</sub> Uptake onto Aerosols Containing Transition Metal ions, *Journal of*  
765 *Physical Chemistry A*, 120, 1421–1430, 10.1021/acs.jpca.5b06316, 2016.

766 Lang, J. L., Zhang, Y. Y., Zhou, Y., Cheng, S. Y., Chen, D. S., Guo, X. U., Chen, S., Li, X. X., Xing, X. F.,  
767 and Wang, H. Y.: Trends of PM<sub>2.5</sub> and Chemical Composition in Beijing, 2000–2015, *Aerosol Air*  
768 *Qual. Res.*, 17, 412–425, 10.4209/aaqr.2016.07.0307, 2017.

769 Li, G., Bei, N., Tie, X., and Molina, L. T.: Aerosol effects on the photochemistry in Mexico City during  
770 MCMA-2006/MILAGRO campaign, *Atmos. Chem. Phys.*, 11, 5169–5182, 10.5194/acp-11-5169-  
771 2011, 2011a.

772 Li, J., Wang, Z., Wang, X., Yamaji, K., Takigawa, M., Kanaya, Y., Pochanart, P., Liu, Y., Irie, H., and Hu,  
773 B.: Impacts of aerosols on summertime tropospheric photolysis frequencies and photochemistry  
774 over Central Eastern China, *Atmos. Environ.*, 45, 1817–1829, 2011b.

775 Li, J., Chen, X. S., Wang, Z. F., Du, H. Y., Yang, W. Y., Sun, Y. L., Hu, B., Li, J. J., Wang, W., Wang, T.,  
776 Fu, P. Q., and Huang, H. L.: Radiative and heterogeneous chemical effects of aerosols on ozone  
777 and inorganic aerosols over East Asia, *Science of the Total Environment*, 622, 1327–1342,  
778 10.1016/j.scitotenv.2017.12.041, 2018.

779 Li, K., Jacob, D. J., Liao, H., Shen, L., Zhang, Q., and Bates, K. H.: Anthropogenic drivers of 2013–  
780 2017 trends in summer surface ozone in China, *Proceedings of the National Academy of Sciences*  
781 *of the United States of America*, 116, 422–427, 10.1073/pnas.1812168116, 2019a.

782 Li, K., Jacob, D. J., Liao, H., Shen, L., Zhang, Q., and Bates, K. H.: Anthropogenic drivers of 2013–  
783 2017 trends in summer surface ozone in China, *Proceedings of the National Academy of Sciences*,  
784 116, 422–427, 2019b.

785 Li, K., Jacob, D. J., Liao, H., Zhu, J., Shah, V., Shen, L., Bates, K. H., Zhang, Q., and Zhai, S.: A two-  
786 pollutant strategy for improving ozone and particulate air quality in China, *Nature Geoscience*, 12,  
787 906–910, 10.1038/s41561-019-0464-x, 2019c.

788 Liu, X., Zhang, Y., Jung, J., Gu, J., Li, Y., Guo, S., Chang, S.-Y., Yue, D., Lin, P., Kim, Y. J., Hu, M., Zeng,  
789 L., and Zhu, T.: Research on the hygroscopic properties of aerosols by measurement and modeling  
790 during CAREBeijing-2006, *Journal of Geophysical Research-Atmospheres*, 114,  
791 10.1029/2008jd010805, 2009.

792 Liu, Z., Wang, Y., Gu, D., Zhao, C., Huey, L. G., Stickel, R., Liao, J., Shao, M., Zhu, T., Zeng, L., Amoroso,  
793 A., Costabile, F., Chang, C. C., and Liu, S. C.: Summertime photochemistry during CAREBeijing-  
794 2007: RO<sub>x</sub> budgets and O<sub>3</sub> formation, *Atmospheric Chemistry and Physics*, 12, 7737–7752,  
795 10.5194/acp-12-7737-2012, 2012.

796 Lou, S. J., Liao, H., and Zhu, B.: Impacts of aerosols on surface-layer ozone concentrations in China  
797 through heterogeneous reactions and changes in photolysis rates, *Atmospheric Environment*, 85,  
798 123–138, 10.1016/j.atmosenv.2013.12.004, 2014.

799 Lu, K., Fuchs, H., Hofzumahaus, A., Tan, Z., Wang, H., Zhang, L., Schmitt, S. H., Rohrer, F., Bohn, B.,  
800 Broch, S., Dong, H., Gkatzelis, G. I., Hohaus, T., Holland, F., Li, X., Liu, Y., Liu, Y., Ma, X., Novelli, A.,  
801 Schlag, P., Shao, M., Wu, Y., Wu, Z., Zeng, L., Hu, M., Kiendler-Scharr, A., Wahner, A., and Zhang,

802 Y.: Fast Photochemistry in Wintertime Haze: Consequences for Pollution Mitigation Strategies,  
803 Environmental Science & Technology, 53, 10676-10684, 10.1021/acs.est.9b02422, 2019.

804 Lu, K. D., Hofzumahaus, A., Holland, F., Bohn, B., Brauers, T., Fuchs, H., Hu, M., Haseler, R., Kita, K.,  
805 Kondo, Y., Li, X., Lou, S. R., Oebel, A., Shao, M., Zeng, L. M., Wahner, A., Zhu, T., Zhang, Y. H., and  
806 Rohrer, F.: Missing OH source in a suburban environment near Beijing: observed and modelled  
807 OH and HO<sub>2</sub> concentrations in summer 2006, Atmospheric Chemistry and Physics, 13, 1057-1080,  
808 10.5194/acp-13-1057-2013, 2013.

809 Lu, X., Hong, J., Zhang, L., Cooper, O. R., Schultz, M. G., Xu, X., Wang, T., Gao, M., Zhao, Y., and  
810 Zhang, Y.: Severe Surface Ozone Pollution in China: A Global Perspective, Environmental Science  
811 & Technology Letters, 5, 487-494, 10.1021/acs.estlett.8b00366, 2018.

812 Ma, Z. Q., Xu, J., Quan, W. J., Zhang, Z. Y., Lin, W. L., and Xu, X. B.: Significant increase of surface  
813 ozone at a rural site, north of eastern China, Atmospheric Chemistry and Physics, 16, 3969-3977,  
814 10.5194/acp-16-3969-2016, 2016a.

815 Ma, Z. W., Hu, X. F., Sayer, A. M., Levy, R., Zhang, Q., Xue, Y. G., Tong, S. L., Bi, J., Huang, L., and Liu,  
816 Y.: Satellite-Based Spatiotemporal Trends in PM<sub>2.5</sub> Concentrations: China, 2004-2013,  
817 Environmental Health Perspectives, 124, 184-192, 10.1289/ehp.1409481, 2016b.

818 Madronich, S.: The atmosphere and UV-B radiation at ground level, in: Environmental UV  
819 photobiology, Springer, 1-39, 1993.

820 Matthews, P. S. J., Baeza-Romero, M. T., Whalley, L. K., and Heard, D. E.: Uptake of  
821 HO<sub>2</sub> radicals onto Arizona test dust particles using an aerosol flow tube, Atmos.  
822 Chem. Phys., 14, 7397-7408, 10.5194/acp-14-7397-2014, 2014.

823 Mihelcic, D., Holland, F., Hofzumahaus, A., Hoppe, L., Konrad, S., Musgen, P., Patz, H. W., Schafer,  
824 H. J., Schmitz, T., Volz-Thomas, A., Bachmann, K., Schlomski, S., Platt, U., Geyer, A., Alicke, B., and  
825 Moortgat, G. K.: Peroxy radicals during BERLIOZ at Pabstthum: Measurements, radical budgets and  
826 ozone production, Journal of Geophysical Research-Atmospheres, 108, 17, 10.1029/2001jd001014,  
827 2003.

828 Monks, P. S., Archibald, A. T., Colette, A., Cooper, O., Coyle, M., Derwent, R., Fowler, D., Granier, C.,  
829 Law, K. S., Mills, G. E., Stevenson, D. S., Tarasova, O., Thouret, V., von Schneidemesser, E.,  
830 Sommariva, R., Wild, O., and Williams, M. L.: Tropospheric ozone and its precursors from the urban  
831 to the global scale from air quality to short-lived climate forcer, Atmospheric Chemistry and  
832 Physics, 15, 8889-8973, 10.5194/acp-15-8889-2015, 2015.

833 Ni, M. J., Huang, J. X., Lu, S. Y., Li, X. D., Yan, J. H., and Cen, K. F.: A review on black carbon emissions,  
834 worldwide and in China, Chemosphere, 107, 83-93, 10.1016/j.chemosphere.2014.02.052, 2014.

835 Parrish, D. D., Xu, J., Croes, B., and Shao, M.: Air quality improvement in Los Angeles-perspectives  
836 for developing cities, Frontiers of Environmental Science & Engineering, 10, 10.1007/s11783-016-  
837 0859-5, 2016.

838 Peeters, J., Nguyen, T. L., and Vereecken, L.: HO<sub>x</sub> radical regeneration in the oxidation of isoprene,  
839 Physical Chemistry Chemical Physics, 11, 5935-5939, 10.1039/b908511d, 2009.

840 Pollack, I. B., Ryerson, T. B., Trainer, M., Neuman, J. A., Roberts, J. M., and Parrish, D. D.: Trends in  
841 ozone, its precursors, and related secondary oxidation products in Los Angeles, California: A  
842 synthesis of measurements from 1960 to 2010, Journal of Geophysical Research-Atmospheres,  
843 118, 5893-5911, 10.1002/jgrd.50472, 2013.

844 Qu, W. J., Wang, J., Zhang, X. Y., Wang, D., and Sheng, L. F.: Influence of relative humidity on  
845 aerosol composition: Impacts on light extinction and visibility impairment at two sites in coastal

846 area of China, *Atmospheric Research*, 153, 500-511, 10.1016/j.atmosres.2014.10.009, 2015.

847 Raga, G. B., Castro, T., and Baumgardner, D.: The impact of megacity pollution on local climate  
848 and implications for the regional environment: Mexico City, *Atmospheric Environment*, 35, 1805-  
849 1811, 10.1016/s1352-2310(00)00275-2, 2001.

850 Real, E., and Sartelet, K.: Modeling of photolysis rates over Europe: impact on chemical gaseous  
851 species and aerosols, *Atmos. Chem. Phys.*, 11, 1711-1727, 10.5194/acp-11-1711-2011, 2011.

852 Shah, V., Jacob, D., Li, K., Silvern, R., Zhai, S., Liu, M., Lin, J., and Zhang, Q.: Effect of changing NOx  
853 lifetime on the seasonality and long-term trends of satellite-observed tropospheric NO<sub>2</sub> columns  
854 over China, 2020.

855 Streets, D. G., Fu, J. S., Jang, C. J., Hao, J. M., and Yu, C.: Air quality during the 2008 Beijing Olympic  
856 Games, *Atmospheric Environment* (1967), 41, 4800-4492, 2007.

857 Taketani, F., Kanaya, Y., and Akimoto, H.: Kinetics of heterogeneous reactions of HO<sub>2</sub> radical at  
858 ambient concentration levels with (NH<sub>4</sub>)<sub>2</sub>SO<sub>4</sub> and NaCl aerosol particles, *The Journal of Physical  
859 Chemistry A*, 112, 2370-2377, 2008.

860 Taketani, F., Kanaya, Y., Pochanart, P., Liu, Y., Li, J., Okuzawa, K., Kawamura, K., Wang, Z., and  
861 Akimoto, H.: Measurement of overall uptake coefficients for HO<sub>2</sub> radicals by aerosol particles  
862 sampled from ambient air at Mts. Tai and Mang (China), *Atmospheric Chemistry and Physics*, 12,  
863 11907-11916, 10.5194/acp-12-11907-2012, 2012.

864 Tan, Z., Fuchs, H., Lu, K., Hofzumahaus, A., Bohn, B., Broch, S., Dong, H., Gomm, S., Häsel, R., He,  
865 L., Holland, F., Li, X., Liu, Y., Lu, S., Rohrer, F., Shao, M., Wang, B., Wang, M., Wu, Y., Zeng, L., Zhang,  
866 Y., Wahner, A., and Zhang, Y.: Radical chemistry at a rural site (Wangdu) in the North China Plain:  
867 observation and model calculations of OH, HO<sub>2</sub> and RO<sub>2</sub> radicals, *Atmos. Chem. Phys.*, 17, 663-  
868 690, 10.5194/acp-17-663-2017, 2017.

869 Tian, R., Ma, X., Jia, H., Yu, F., Sha, T., and Zan, Y.: Aerosol radiative effects on tropospheric  
870 photochemistry with GEOS-Chem simulations, *Atmospheric Environment*, 208, 82-94, 2019.

871 Verstraeten, W. W., Neu, J. L., Williams, J. E., Bowman, K. W., Worden, J. R., and Boersma, K. F.:  
872 Rapid increases in tropospheric ozone production and export from China, *Nature geoscience*, 8,  
873 690, 2015.

874 Wang, B., Shao, M., Lu, S. H., Yuan, B., Zhao, Y., Wang, M., Zhang, S. Q., and Wu, D.: Variation of  
875 ambient non-methane hydrocarbons in Beijing city in summer 2008, *Atmospheric Chemistry and  
876 Physics*, 10, 5911-5923, 10.5194/acp-10-5911-2010, 2010.

877 Wang, H., Lu, K., Tan, Z., Sun, K., Li, X., Hu, M., Shao, M., Zeng, L., Zhu, T., and Zhang, Y.: Model  
878 simulation of NO<sub>3</sub>, N<sub>2</sub>O<sub>5</sub> and ClNO<sub>2</sub> at a rural site in Beijing during CAREBeijing-2006,  
879 *Atmospheric Research*, 196, 97-107, 2017.

880 Wang, J., Allen, D. J., Pickering, K. E., Li, Z., and He, H.: Impact of aerosol direct effect on East Asian  
881 air quality during the EAST-AIRE campaign, *Journal of Geophysical Research: Atmospheres*, 121,  
882 6534-6554, 2016a.

883 Wang, J. L., Din, G. Z., and Chan, C. C.: Validation of a laboratory-constructed automated gas  
884 chromatograph for the measurement of ozone precursors through comparison with a commercial  
885 analogy, *Journal of Chromatography A*, 1027, 11-18, 10.1016/j.chroma.2003.08.099, 2004.

886 Wang, M., Zeng, L., Lu, S., Shao, M., Liu, X., Yu, X., Chen, W., Yuan, B., Zhang, Q., Hu, M., and Zhang,  
887 Z.: Development and validation of a cryogen-free automatic gas chromatograph system (GC-  
888 MS/FID) for online measurements of volatile organic compounds, *Analytical Methods*, 6, 9424-  
889 9434, 10.1039/c4ay01855a, 2014.

890 Wang, M., Shao, M., Chen, W., Lu, S., Liu, Y., Yuan, B., Zhang, Q., Zhang, Q., Chang, C. C., Wang, B.,  
891 Zeng, L., Hu, M., Yang, Y., and Li, Y.: Trends of non-methane hydrocarbons (NMHC) emissions in  
892 Beijing during 2002-2013, *Atmospheric Chemistry and Physics*, 15, 1489-1502, 10.5194/acp-15-  
893 1489-2015, 2015a.

894 Wang, P., Wang, T., and Ying, Q.: Regional source apportionment of summertime ozone and its  
895 precursors in the megacities of Beijing and Shanghai using a source-oriented chemical transport  
896 model, *Atmos. Environ.*, 224, 10, 10.1016/j.atmosenv.2020.117337, 2020.

897 Wang, Q. Q., Sun, Y. L., Jiang, Q., Du, W., Sun, C. Z., Fu, P. Q., and Wang, Z. F.: Chemical composition  
898 of aerosol particles and light extinction apportionment before and during the heating season in  
899 Beijing, China, *Journal of Geophysical Research-Atmospheres*, 120, 12708-12722,  
900 10.1002/2015jd023871, 2015b.

901 Wang, W., Li, X., Shao, M., Hu, M., Zeng, L., Wu, Y., and Tan, T.: The impact of aerosols on photolysis  
902 frequencies and ozone production in Beijing during the 4-year period 2012-2015, *Atmos. Chem.*  
903 *Phys.*, 19, 9413-9429, 10.5194/acp-19-9413-2019, 2019.

904 Wang, X. M., Chen, W. H., Chen, D. H., Wu, Z. Y., and Fan, Q.: Long-term trends of fine particulate  
905 matter and chemical composition in the Pearl River Delta Economic Zone (PRDEZ), China, *Front.*  
906 *Env. Sci. Eng.*, 10, 53-62, 10.1007/s11783-014-0728-z, 2016b.

907 Wang, Y., Zhang, Y., Hao, J., and Luo, M.: Seasonal and spatial variability of surface ozone over  
908 China: contributions from background and domestic pollution, *Atmospheric Chemistry and Physics*,  
909 11, 3511-3525, 10.5194/acp-11-3511-2011, 2011.

910 Warneke, C., de Gouw, J. A., Holloway, J. S., Peischl, J., Ryerson, T. B., Atlas, E., Blake, D., Trainer, M.,  
911 and Parrish, D. D.: Multiyear trends in volatile organic compounds in Los Angeles, California: Five  
912 decades of decreasing emissions, *Journal of Geophysical Research-Atmospheres*, 117,  
913 10.1029/2012jd017899, 2012.

914 Wehner, B., Birmili, W., Ditas, F., Wu, Z., Hu, M., Liu, X., Mao, J., Sugimoto, N., and Wiedensohler,  
915 A.: Relationships between submicrometer particulate air pollution and air mass history in Beijing,  
916 China, 2004-2006, *Atmospheric Chemistry and Physics*, 8, 6155-6168, 10.5194/acp-8-6155-2008,  
917 2008.

918 Wendisch, M., Mertes, S., Ruggaber, A., and Nakajima, T.: Vertical profiles of aerosol and radiation  
919 and the influence of a temperature inversion: Measurements and radiative transfer calculations, *J.*  
920 *Appl. Meteorol.*, 35, 1703-1715, 10.1175/1520-0450(1996)035<1703:vpoaar>2.0.co;2, 1996.

921 Xie, X., Shao, M., Liu, Y., Lu, S., Chang, C.-C., and Chen, Z.-M.: Estimate of initial isoprene  
922 contribution to ozone formation potential in Beijing, China, *Atmospheric Environment*, 42, 6000-  
923 6010, 10.1016/j.atmosenv.2008.03.035, 2008.

924 Xing, J., Wang, J., Mathur, R., Wang, S., Sarwar, G., Pleim, J., Hogrefe, C., Zhang, Y., Jiang, J., and  
925 Wong, D. C.: Impacts of aerosol direct effects on tropospheric ozone through changes in  
926 atmospheric dynamics and photolysis rates, *Atmospheric chemistry and physics*, 17, 9869, 2017.

927 Xu, J., Ma, J. Z., Zhang, X. L., Xu, X. B., Xu, X. F., Lin, W. L., Wang, Y., Meng, W., and Ma, Z. Q.:  
928 Measurements of ozone and its precursors in Beijing during summertime: impact of urban plumes  
929 on ozone pollution in downwind rural areas, *Atmospheric Chemistry and Physics*, 11, 12241-12252,  
930 10.5194/acp-11-12241-2011, 2011.

931 Xu, J., Zhang, Y. H., Zheng, S. Q., and He, Y. J.: Aerosol effects on ozone concentrations in Beijing:  
932 A model sensitivity study, *J. Environ. Sci.*, 24, 645-656, 10.1016/s1001-0742(11)60811-5, 2012.

933 Yuan, B., Shao, M., de Gouw, J., Parrish, D. D., Lu, S., Wang, M., Zeng, L., Zhang, Q., Song, Y., Zhang,

934 J., and Hu, M.: Volatile organic compounds (VOCs) in urban air: How chemistry affects the  
935 interpretation of positive matrix factorization (PMF) analysis, *Journal of Geophysical Research-*  
936 *Atmospheres*, 117, 10.1029/2012jd018236, 2012.

937 Zhang, J. P., Zhu, T., Zhang, Q. H., Li, C. C., Shu, H. L., Ying, Y., Dai, Z. P., Wang, X., Liu, X. Y., Liang,  
938 A. M., Shen, H. X., and Yi, B. Q.: The impact of circulation patterns on regional transport pathways  
939 and air quality over Beijing and its surroundings, *Atmospheric Chemistry and Physics*, 12, 5031-  
940 5053, 10.5194/acp-12-5031-2012, 2012.

941 Zhang, L., Shao, J. Y., Lu, X., Zhao, Y. H., Hu, Y. Y., Henze, D. K., Liao, H., Gong, S. L., and Zhang, Q.:  
942 Sources and Processes Affecting Fine Particulate Matter Pollution over North China: An Adjoint  
943 Analysis of the Beijing APEC Period, *Environ. Sci. Technol.*, 50, 8731-8740, 10.1021/acs.est.6b03010,  
944 2016.

945 Zhang, Q., Yuan, B., Shao, M., Wang, X., Lu, S., Lu, K., Wang, M., Chen, L., Chang, C. C., and Liu, S.  
946 C.: Variations of ground-level O<sub>3</sub> and its precursors in Beijing in summertime between 2005 and  
947 2011, *Atmospheric Chemistry and Physics*, 14, 6089-6101, 10.5194/acp-14-6089-2014, 2014.

948 Zhao, B., Wang, S. X., Liu, H., Xu, J. Y., Fu, K., Klimont, Z., Hao, J. M., He, K. B., Cofala, J., and Amann,  
949 M.: NO<sub>x</sub> emissions in China: historical trends and future perspectives, *Atmospheric Chemistry and*  
950 *Physics*, 13, 9869-9897, 10.5194/acp-13-9869-2013, 2013.

951 Zhao, P. S., Zhang, X. L., and Xu, X. F.: Long-term visibility trends and characteristics in the region  
952 of Beijing, Tianjin, and Hebei, China, *Abstr. Pap. Am. Chem. Soc.*, 242, 1, 2011.

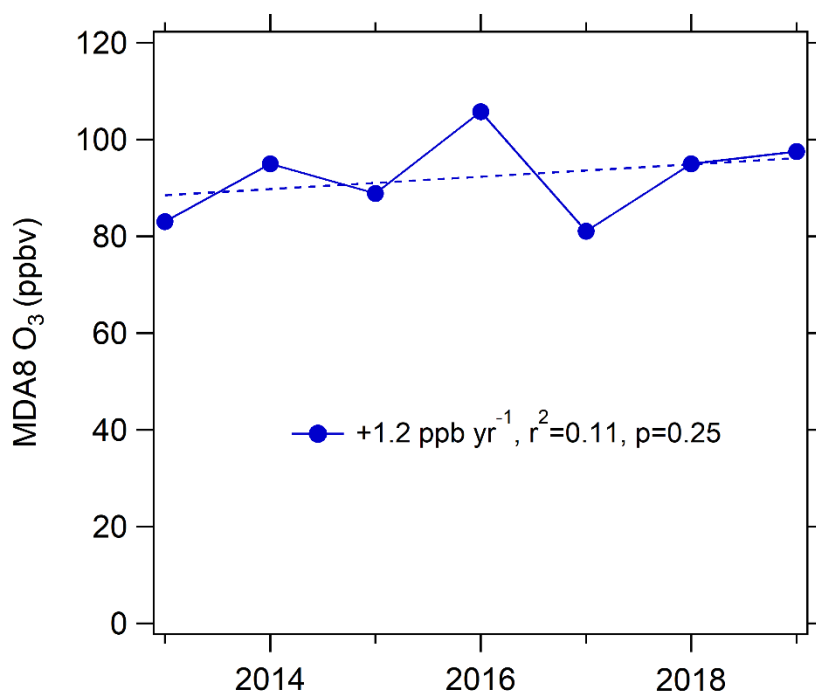
953 Zheng, C., Zhao, C., Zhu, Y., Wang, Y., Shi, X., Wu, X., Chen, T., Wu, F., and Qiu, Y.: Analysis of  
954 influential factors for the relationship between PM<sub>2.5</sub> and AOD in Beijing, *Atmospheric*  
955 *Chemistry and Physics*, 17, 13473-13489, 2017.

956 Zou, Q., Song, H., Tang, M., and Lu, K.: Measurements of HO<sub>2</sub> uptake coefficient on aqueous  
957 (NH<sub>4</sub>)<sub>2</sub>SO<sub>4</sub> aerosol using aerosol flow tube with LIF system, *Chin. Chem. Lett.*, 30, 2236-2240,  
958 <https://doi.org/10.1016/j.ccllet.2019.07.041>, 2019.

959

960

961



963

964 Figure S1. The trend of average MDA8 ozone in Changdao during 2013-2019. These  
 965 data are acquired from “Blue book on prevention and control of atmospheric ozone  
 966 pollution in China (in Chinese)” reported by Chinese Society of Environmental  
 967 Sciences in 2020  
 968 ([http://www.epserve.com/forepart/zxnr\\_index.do?oid=51478637&tid=26378242](http://www.epserve.com/forepart/zxnr_index.do?oid=51478637&tid=26378242)).

969

970

971

972

973

974

975

976

977

978

979

980

981

982

983

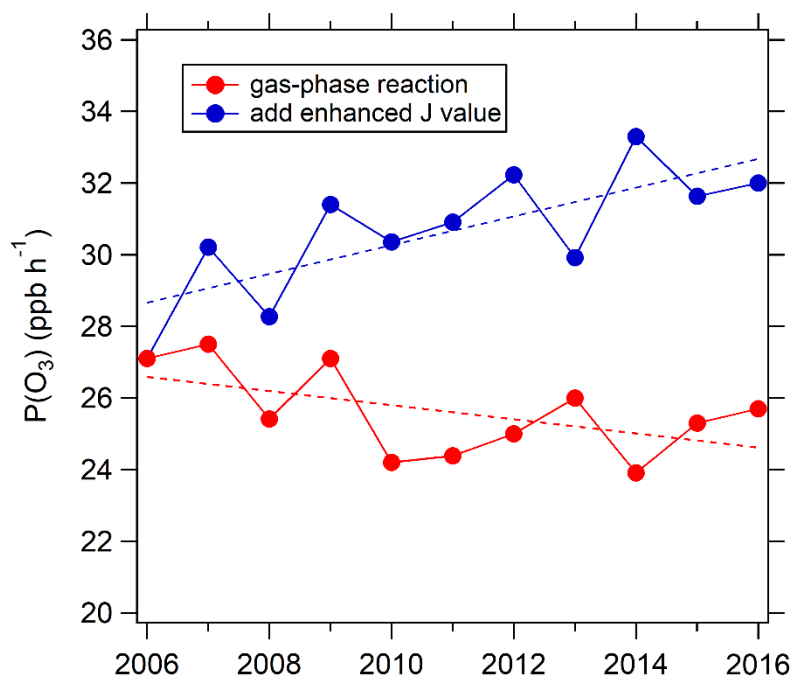
984

985

986

987

988



990

991 Figure S2. Trend of monthly afternoon (12:00-15:00) mean  $P(O_3)$  simulated by the  
992 chemical box model. Red dots: Only the gas-phase reactions are considered in the box  
993 model constrained by observed photolysis frequencies from 2006 for all eleven years.  
994 Blue dots: the box model as above, but constrained by the photolysis frequencies  
995 derived for each year without the changing aerosol uptake of  $HO_2$  considered.

996

997

998

999

1000

1001

1002

1003

1004

1005

1006

1007

1008

1009

1010

1011

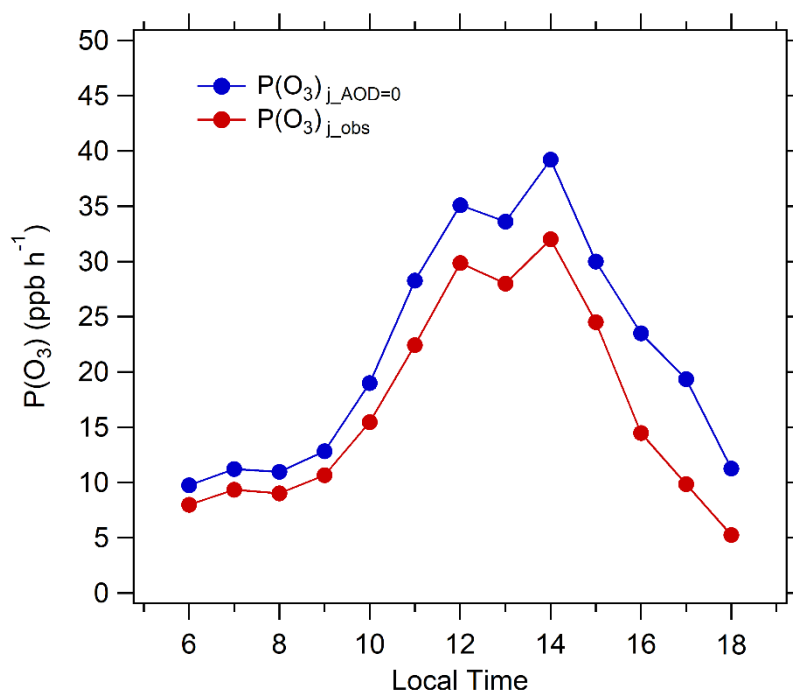
1012

1013

1014

1015

1016



1017

1018 Figure S3. Diurnal variation of simulated P(O<sub>3</sub>) in Beijing in August during 2005-

1019 2016. P(O<sub>3</sub>)<sub>j\_obs</sub> represents ozone production rate under observed photolysis

1020 frequencies; P(O<sub>3</sub>)<sub>j\_AOD=0</sub> represents ozone production rate under calculated

1021 photolysis frequencies when AOD is equal to 0.